

1.2 Scientific Goals and Objectives.

Key elements of NASA's Sun-Earth Connections theme are SECCHI primary goals

- What configuration of the corona leads to a CME?
- What initiates a CME?
- What accelerates CMEs?
- How does a CME interact with the heliosphere?
- How do CMEs cause space weather disturbances?

Coronal mass ejections (CMEs) are spectacular demonstrations of solar activity. Despite nearly thirty years of observations, the basic physics that expels these plasma clouds into the heliosphere is still not well understood. The proposed SECCHI suite is designed to explore various manifestations of the CME process. The role of the magnetic field development in the photosphere and corona and its coupling to the propagation and acceleration processes is crucial to a fuller understanding of these geo-effective dynamic events. The strength of the STEREO mission, combining comparable observations from two distinct views, is perfectly suited to the exploration of all of the manifestations of CMEs, both at the source and during their propagation to 1 AU.

The STEREO spacecraft will separate at a rate of about 45 degrees per year, thereby providing two distinct and unique approaches to understanding the key physics leading to CMEs. Early in the mission both STEREO spacecraft will view the same features in the corona on a variety of scales. Later in the mission, STEREO will provide unique perspectives of the CME process from widely separated viewpoints. SECCHI takes full advantage of these capabilities to improve dramatically on our existing knowledge of the eruptive process. SOHO has demonstrated the necessity for observing CMEs over a large range of spatial scales (e.g., Dere et al. 1997). The SECCHI instruments provide comprehensive coverage of the full range of spatial and temporal scales required to observe the buildup, initiation, and evolution of CMEs, from the surface magnetic field through the EUV emitting low corona, to the large-scale corona, and heliosphere, from cradle to grave.

1.2.1 The Magnetic Origin of CMEs.

Key Observational Questions

- How is the requisite energy storage achieved and how is it released?
- Does the CME process require magnetic complexity (e.g., multi-flux system)?
- Is a magnetic topology flux rope a necessary pre-CME configuration?
- What form does any complexity take?

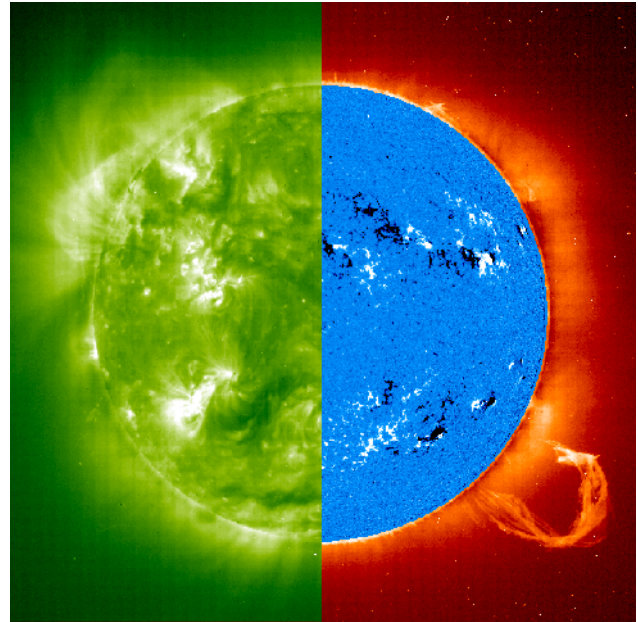


Figure 1-1.

Left, EIT 195Å image of the corona, right disk, MDI magnetogram. Right, EIT 304Å image of transition region structures including an eruptive prominence.

All forms of solar activity arise from the interplay between plasmas and magnetic fields. The positions of the plasma loops seen in Figure 1-1, reflect the continuity of the magnetic field lines that connect photospheric regions of positive magnetic polarity with regions of negative polarity. CMEs have a strong correlation with eruptive prominences that are often embedded at the base of streamers and frequently display the classical 3-part CME structure: a bright frontal loop surrounding a dark cavity containing a bright core (Illing & Hundhausen, 1985). One of the first CMEs observed in the EUV by EIT showed such a 3-part structure at a very early stage of its development (Figure 1-2). CMEs originate in the magnetic fields of the corona, and in the free energy stored in these magnetic fields.

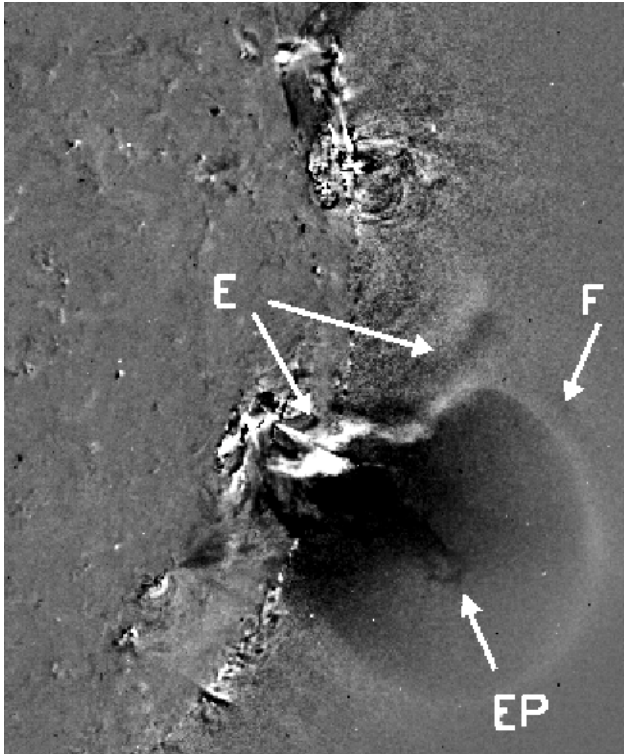


Figure 1-2. EIT observations of a CME with 3 part structure on 1996 Dec. 23

□ *Magnetic Structure:* Changes in the pre-CME magnetic configuration are an important aspect of the CME eruption process. Feynman and Martin (1995) have demonstrated the role of newly emerging magnetic flux in the initiation of eruptive prominences and Feynman (1997) suggests that CMEs are the result of the dynamics of ‘evolving magnetic structures’ on a variety of scales. The ability to determine the behavior of the surface magnetic field in the evolving footpoint structures is crucial to determine the physics of CMEs.

For example, the principal mechanism invoked for converting the free energy in the magnetic field into kinetic and thermal energy is magnetic reconnection. To understand observations of apparent reconnection and how they relate to the CME, we must know the initial coronal magnetic field configuration. Is it potential, force-free, or in a more complex and energetic state? SECCHI will answer this question by comparing models of the coronal fields, force-free or full 3D MHD derived from VMAG photospheric *vector* magnetograms, with EUVI images of coronal loops.

A complete 3D specification of the observed coronal loop structure is required to understand the

coronal field configuration. Knowledge of the coronal magnetic configuration before, during and after the eruption of a CME will address questions relevant to the initiation and evolution of the CME as it propagates out into interplanetary space. Aschwanden et al. (1999) demonstrated the technique of “dynamic stereoscopy” which is capable of providing this information. This is demonstrated in Figure 1-3, which shows the potential field compared with the 3D positions of coronal loops observed in various EIT channels. This technique is limited, however, in its ability to distinguish time varying structures. The use of simultaneous EUVI image pairs will dramatically improve the accuracy of these techniques.

An important result from observations of the pre-CME corona using *Yohkoh/SXT* is that sigmoidal loop structures are predictors of major eruptions (Canfield et al., 1999). These sigmoidal structures are, in turn, thought to result from concentrations of magnetic helicity in the corona. To observe the formation of the helicity loaded structures and to understand the relation between magnetic helicity and CME initiation requires coincident observations of photospheric vector magnetic fields and the coronal loop manifestations of this phenomenon. Joint EUV observations, of the highest temperature line, and vector magnetic observations are key elements of the SECCHI science package since the helicity can only be observed with vector capability. With stereoscopic viewing, the helicity buildup and CME initiation will be observed from the spacecraft looking directly down on the CME where the vector magnetic field measurements are most reliable, while the resulting CME and coronal structure will be observed stereoscopically from both viewpoints. It is the broad longitudinal coverage of the vector magnetographs from the two spacecraft that makes this observation possible.

□ *Energetics:* The Aly-Sturrock conjecture (Aly, 1984; Sturrock, 1991) implies that a closed magnetic field has less energy than the equivalent fully open field, with the same photospheric boundary condition. This severely constrains the occurrence of a CME in a force-free corona if the magnetic field is the primary driver of the eruption. There are three physical approaches to CME production that satisfy this constraint: (1) the pre-CME magnetostatic corona is not force-free and cross-field currents are present (Wolfson & Dlamini, 1997);

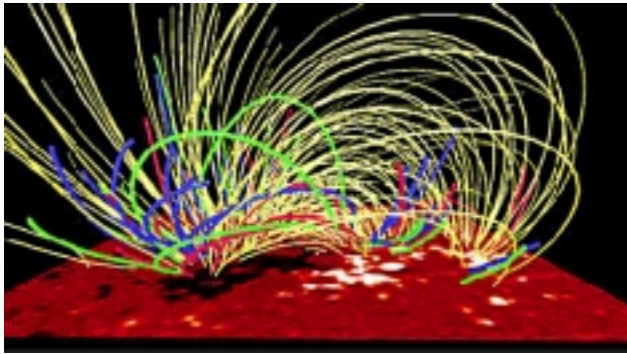


Figure 1-3. Yellow: potential field lines, Blue: EIT 171A, Green: EIT 195A, Red: 284A

(2) the CME involves flux from several flux systems so that most of the field involved is not opened (Antiochos, DeVore & Klimchuk, 1997); (3) the CME includes a detached flux rope (Low, 1996).

Photospheric vector magnetograms from SECCHI will explain the energetics of CMEs both by mapping the magnetic shear and magnetic neutral lines over a large fraction of the solar surface and by estimation of the available magnetic free energy. Since the observed photospheric field is unlikely to be force-free (Metcalf et al., 1995), extrapolation of the vector field is unlikely to provide sufficient information on the coronal magnetic structure and energetics prior to CME onset. To make progress, the magnetic morphology in the corona, observed over a broad temperature range with the EUVI telescope, must be combined with the photospheric magnetic field measurements, as an

additional boundary condition for the extrapolations.

Techniques combining the photospheric field with observed coronal structures give a consistent picture of the coronal magnetic energy storage. Such techniques are available and will be applied to SECCHI. For example, a semi-empirical magnetic extrapolation technique has recently been developed by Gary and Alexander (1999) and applied successfully to the combination of line-of-sight magnetograms and *Yohkoh/SXT* images. In this technique, a potential field extrapolation is stretched radially so that calculated and observed structures match. The 3D field thus generated includes cross-field currents which are not directly observable from the photospheric magnetograms.

The semi-empirical method is currently limited by the lack of information on the 3D structure of the corona. Simultaneous and well-separated views from the EUVI telescope, with its broad temperature coverage, will overcome this limitation.

□ *Instrument Requirements to Observe Magnetic Origins of CMEs:* The vector magnetic fields observed with VMAG provide for extrapolation into the corona and for predicting the global magnetic structure. While the finest scale magnetic structures will not be visible, Aulanier (in Van Driel and Martinez-Pillet, 1999) has demonstrated that much of the global topology of the large-scale magnetic field is insensitive to the spatial resolution of the magnetograph. Required instrument parameters are shown in Table 1-1.

Table 1-1. Magnetic Origin of CMEs: Instrumental Requirements

Inst.	FOV	Cadence	Resolution	Comment
VMAG	Full-disk	2 per hour	4"	<ul style="list-style-type: none"> ▪ 30 min resolution shows large scale magnetic evolution and slow energy buildup.
EUVI	Full-disk	2 per hour	3"	<ul style="list-style-type: none"> ▪ Resolution better than EIT to observe loop structure. ▪ Broad coronal temperature sensitivity.
COR1	4R _☉	1 per hour	8"	<ul style="list-style-type: none"> ▪ Polarization brightness for high contrast
COR2	15R _☉	1 per hour	30"	<ul style="list-style-type: none"> ▪ pB and B for 3D structure along LOS

1.2.2 The Initiation of CMEs.

Key Observational Questions

- Are coronal cavities ubiquitous?
- What is the role of coronal dimming?
- Is magnetic complexity necessary?
- Is there evidence of interactions of flux systems?
- Is there evidence for reconnection?

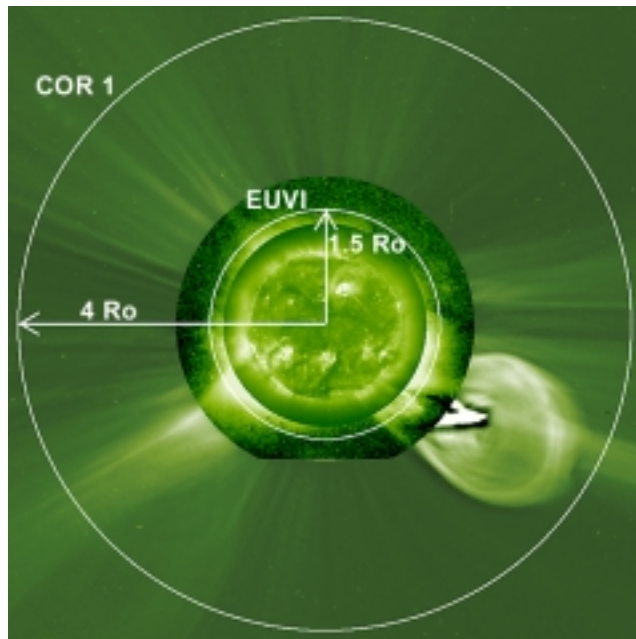


Figure 1-4

A primary science goal of STEREO is the determination of the mechanism for CME initiation. This would constitute a major breakthrough in understanding the fundamental causes of solar activity.

Observations with SOHO have revealed that the initiation of a CME is evident on both very small and very large spatial scales. The first CME well-observed with the EIT (Dere et al., 1997) showed (Figure 1-5) that the initiation came with the rapid eruption of a small 5x35" portion of prominence material (EP) accompanied by a small brightening observable as a weak X-ray (class B2) flare. The LASCO coronagraph observed the typical slow brightening (B) and swelling of the large overlying helmet streamer leading up to the CME.

Several possible theoretical scenarios for CME initiation have been proposed but few have been ruled out. Low (1996) has suggested that a CME is the eruption of a magnetic flux rope that is gravitationally confined within a helmet streamer cavity because of the cool, dense prominence material.

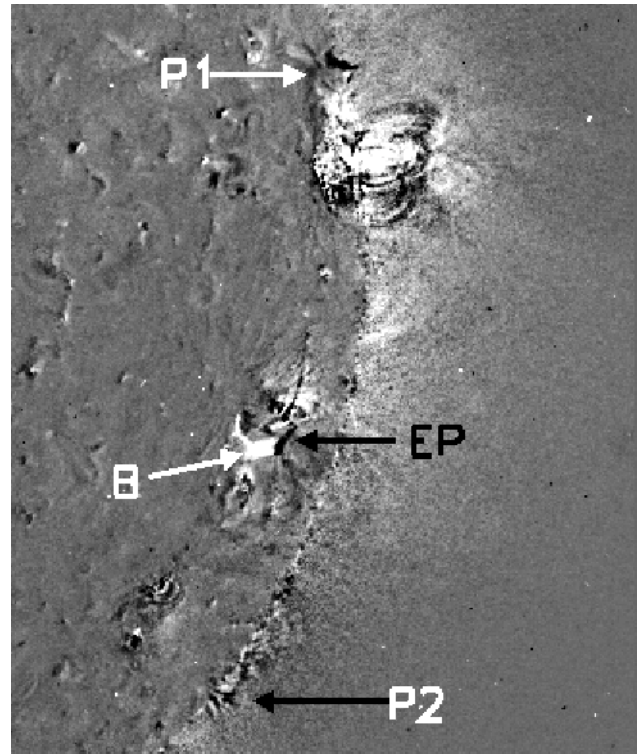


Figure 1-5. EIT running difference image at the initiation of the 1996 December 23 CME

Once this material drains, the flux rope becomes buoyant, rises, and erupts by pushing aside the helmet streamer field line. LASCO observations indicate that a significant number of CMEs are apparently consistent with a magnetic flux rope topology (Chen et al., 1997; Dere et al., 1999). MHD simulations by Wu et al. (1997) find that a flux rope with sufficient magnetic or plasma energy density will erupt in a manner similar to that proposed by Low. The source of this energy is currently unknown.

Recently, Antiochos et al. (1999) have suggested that multiple magnetic flux systems are a key element in CME initiation. In this model, reconnection removes unstressed magnetic flux that overlies the highly stressed core field and, thereby, allows the core field to erupt. On the other hand Moore and Roumeliotis (1992) suggest that magnetic reconnection occurs low down, below the stressed field region.

Theories of CMEs are not always well related to observational signatures. These signatures include the eruption of cool prominence material, the rapid motion of wispy coronal features, foot-point dimming (Hudson et al., 1998), and coronal

EIT waves (Thompson et al., 1999). Observations with the LASCO C1 coronagraph suggest that CMEs undergo strong structural changes in the 1.1 to 3 R_{\odot} range (Dere et al., 1999). A verification of any of the theoretical models requires that we understand the three dimensional structure of the magnetic field configuration that gives rise to the CME and how this configuration evolves. The primary signature of magnetic reconnection is that a new magnetic field line topology develops. This should be evident in new magnetic connections of coronal plasma loops. Because of the confusion of structures along the line-of-sight, this has not been possible from a single viewpoint and requires STEREO observations to elucidate the three dimensional structure.

When the two spacecraft are less than about 45 degrees separation, sequences of stereo image pairs can be viewed “three dimensionally” using stereoscopic methods. We will use advanced stereoscopic digital techniques and technologies to display and analyze sequences of stereo image pairs. Available techniques will provide the observer with qualitative but excellent perceptions of 3D coronal and CME structures. These serve as a starting point for quantitative analyses that will compare STEREO observations with detailed 3D theoretical models.

Required instrumental parameters are shown in Table 1-2. While in general we desire a rapid cadence in the EUVI and COR1 instruments, certain slow, large-scale coronal changes are also a clue to initiation. For example, the slow swelling of a helmet streamer (the ‘bugle’ pattern) is often a precursor, by several hours, of a CME eruption, and can be explored with synoptic VMAG and COR1 observations.

We have considered implementing EUV Doppler velocity imaging. Coronal Doppler velocities could provide useful information during the CME initiation, while chromospheric Doppler velocities

Table 1-2. Initiation of CMEs: Instrumental Requirements

Inst.	FOV	Cadence	Resolution	Comment
VMAG	Full-disk	3 per hour	4"	Full disk to catch events; 20 min resolution shows build-up of shear; small-scale (6-8") flux turns over on ~40-minute time scale.
EUVI	Full-disk	1 per min.	6"	171 Å/195Å and 304Å to show fast evolution of coronal loops and filaments
COR1	4 R_{\odot}	5 min.	16"	Will observe CME as it accelerates through the field-of-view
COR2	15 R_{\odot}	1 per 20 min.	30"	Observe CME acceleration and LOS extent

would show fast flows in erupting filaments. Technically, Doppler imaging is feasible with the current EUVI design. Two spectral channels would observe in the blue and red wings of an emission line.

The ratio of the two intensities is a measure of the line-of-sight velocity. Temperature and density variations of lines within the instrument pass-band introduce spurious Doppler signals, as observed by the Japanese XDT rocket experiment. Extensive calculations have shown that state-of-the-art EUV coating technology (0.2 mm FWHM) and a careful line choice (e.g., 17.1 nm) reduce those spurious signals to 20-30 km/s (1-sigma). However, Doppler imaging works well only for bright objects, and, in the chromospheric He 30.4 nm line, only for objects off the limb.

Because of its limitations, and since it comes at the scientific cost of coronal temperature coverage, Doppler imaging is not included in the instrument baseline. During phase A, the STEREO science team will reconsider Doppler imaging, since its implementation would not add to cost, mass, power, or schedule, but only be a matter of scientific trade-off.

1.2.3 Physical Evolution of CMEs.

Key Observational Questions

- What is the 3D structure of CMEs?
- What is the relationship between the local and global corona?
- What is the role of reconnection?
- How is a CME accelerated?
- What is the low corona response to CMEs?

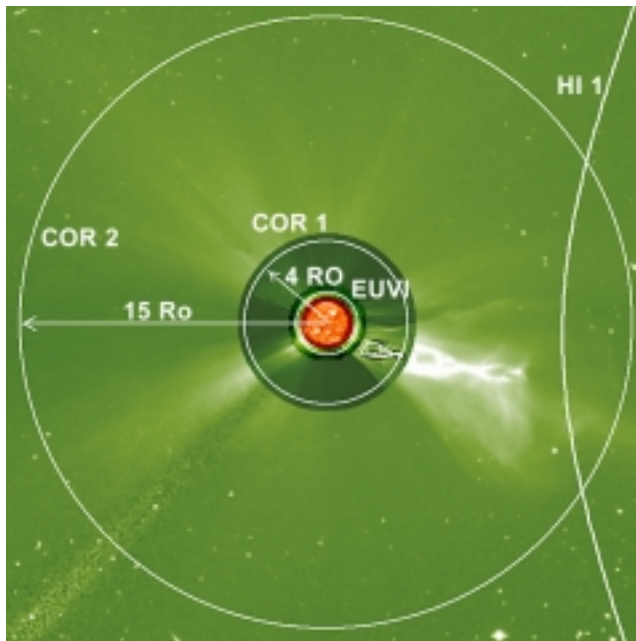


Figure 1-6

Our present knowledge of the size of CMEs has been limited to direct observations of the projection of their angular spans and their radial extent. While this has provided good estimates of their latitudinal and radial extents, we have no direct knowledge of the longitudinal size of these structures. This is one of the fundamental questions that STEREO observations will address.

After initiation, CMEs continue to have a profound effect on the solar atmosphere. They play a central role in the long-term evolution of the structure of the solar corona (Hundhausen, 1995) and are the prime link between solar activity and large, transient interplanetary and geomagnetic disturbances (Gosling, 1993). The physical evolution of the various CME manifestations yields crucial information on the nature and properties of these events, from their initial ejection to their eventual demise in the outer reaches of the heliosphere.

Observations by LASCO have confirmed the existence of two classes of CMEs (Howard, 1999)

as determined by their velocity profiles as they propagate through the corona. MacQueen and Fisher (1983) observed that some CMEs started at a high speed and continued outward with little or no acceleration while others started slowly and accelerated. LASCO observes acceleration as high as 30 m/s^2 and speeds as high as 2000 km/s . What supplies the force for this continued acceleration out to $30 R_{\odot}$?

A recent study (Vourlidis et al., 1999) indicates that some of the accelerating flux rope CMEs have constant total energy: magnetic plus kinetic plus potential. Figure 1-7 shows that magnetic energy is being transferred to kinetic energy. Other flux rope CMEs have increasing total energy, indicating that some external force continues to act on the CME. Thus the energetics of the CME are defined both low in the solar atmosphere and higher up. Determining the source of the CME energy requires the full range of solar atmospheric observations provided by SECCHI.

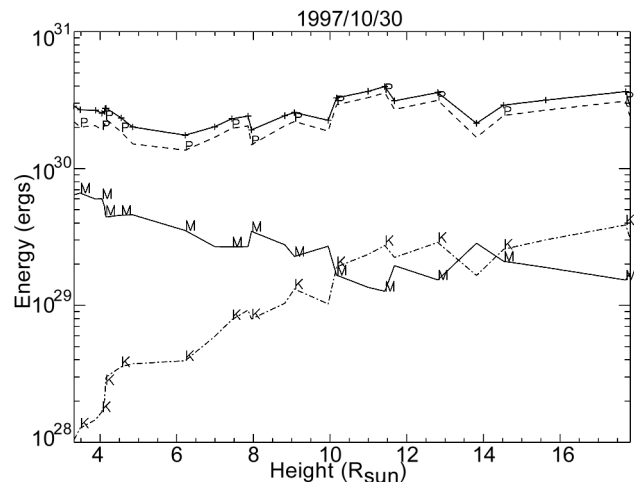


Figure 1-7. Total (solid line), potential (P), kinetic (K) and magnetic energy (M) for a flux rope type CME

The recent discovery of waves in the EUV corona by EIT (Thompson, 1999) are another aspect of the complex nature of the CME phenomenon. These coronal density enhancements associated with the CME, propagate across the solar disk at speeds of $200\text{-}300 \text{ km/s}$. Figure 1-8 shows an example of a bright EIT wave that originated from the active region in the SE that produced a flare and a halo CME. The separate perspectives afforded by the two sets of SECCHI instruments adds critical information about the dynamic evolution of the magnetic field, the propagation of the wave

through the corona, the dimming of hot plasma in the low corona, and evolution of the CME as it progresses through the large-scale corona.

The required instrument parameters are shown in Table 1-3.

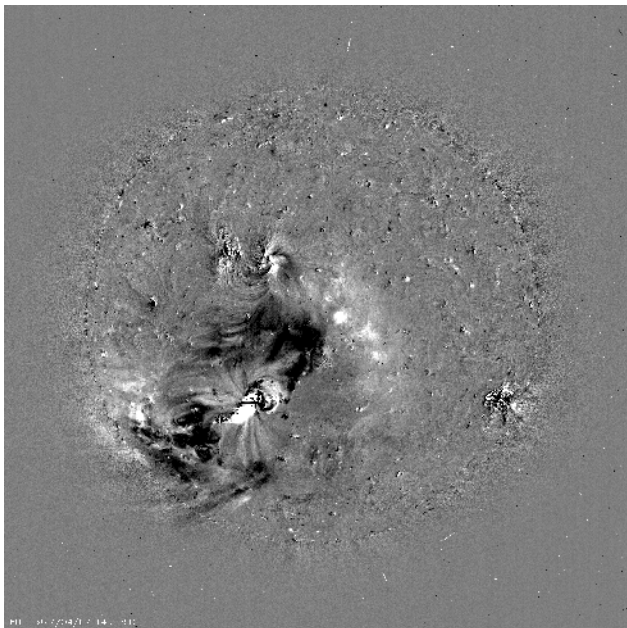


Figure 1-8. EIT observations of a coronal wave emitted following a flare and a CME

Table 1-3. Physical Evolution of CMEs: Instrumental Requirements

Inst.	FOV	Cadence	Resolution	Comment
EUVI	Full-disk	10 per hour	6"	Full disk to cover events; all wavelengths (171Å, 195Å, 211 Å, 304 Å) on a 8-minute cadence to observe formation of post-CME arcade. Observe coronal waves.
COR1	4R _☉	3 per hour	16"	Observe morphological development of the post-CME Helmet streamer and the middle corona.
COR2	15R _☉	3 per hour	30"	Observe passage of CME through the inner heliosphere

1.2.4 CME Interaction with Heliosphere.

Key Observational Questions

- What is the relationship between the CME and interplanetary phenomena?
- What is the 3D structure of magnetic clouds?
- Where and how are particles accelerated in the heliosphere?
- Where and why do the fast CMEs decelerate to the solar wind speeds?

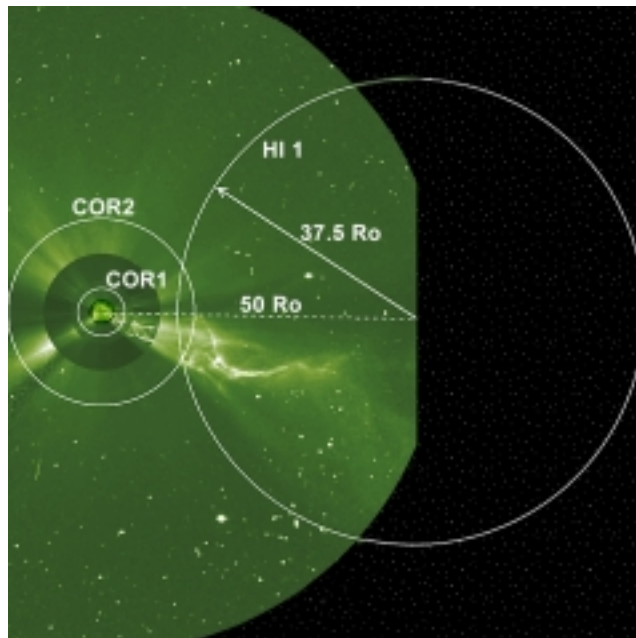


Figure 1-9. Extrapolated expansion of a CME into the HI-1 FOV

The STEREO spacecraft will provide the first platform for making the kinds of coordinated global measurements of heliospheric events and structures that have been possible on only a handful of occasions in the entire history of spaceflight. VMAG provides the photospheric magnetic field information that is the basis for the heliospheric field patterns that are then modified by solar wind flow fields and CMEs (Linker & Mikic, 1995). EUVI, COR1, and COR2 observe the coronal configuration at the base of the heliosphere while the HI images the density enhancements of CMEs and the heliospheric plasma sheet out to 1 AU. For the first time these measurements, combined with the particle and field observations, will provide an observational basis for the complex interaction of heliospheric structures.

At present, the basic structure of a CME near the Sun is well known: a large, bright object that

expands as it propagates away from the Sun at speeds between 50 and 2000 km/s. Our knowledge of CME structure near 1 AU is much poorer, largely due to the lack of image data to augment *in situ* observations. Interplanetary ejecta measured *in situ* at 1 AU are characterized by strong magnetic fields, weak magnetic field fluctuations, low proton β , low proton temperature, enhanced helium abundance, bi-directional non-thermal electron streaming, and bi-directional proton streaming (Zwickl, 1983). These signatures rarely coexist in a given event, however, and even when two or more of these signatures are present there generally is no consistent temporal association among them (Galvin, 1997; Neugebauer & Goldstein, 1977). Some ejecta have been identified as magnetic clouds (Burlaga et al., 1981) but not all CMEs are likely to evolve into magnetic clouds (Kahler et al., 1999). Because ejecta cannot be identified uniquely at 1 AU, it is not surprising that the relation between interplanetary ejecta and CMEs has proven difficult to understand.

Combining the complementary remote sensing and *in situ* measurements will provide unprecedented comprehensive views of the evolving CME structure. The SECCHI coronagraphs and HI remotely measure the global electron density structure of a CME, while the *in situ* particle and fields experiment make comprehensive measurements of the local plasma parameters, density, temperature, magnetic field strength, and orientation. When the separation between the two STEREO spacecraft is roughly 30 degrees or larger, the coronagraphs and HI on one STEREO spacecraft will be able to observe CMEs that will impact the other spacecraft. As the CME passes over one spacecraft, the particle and fields experiment will record the local parameters while simultaneous observations from the SECCHI imagers on the other spacecraft determine where in the CME the *in situ* measurements are made.

This innovative approach will avoid past difficulties in deriving the global structure of heliospheric disturbances from either *in situ* or remote observations alone, and it should resolve present uncertainties regarding the interplanetary manifestations of CMEs. One important issue that will be addressed is whether the derived 3D magnetic configuration is a flux rope or another type of structure, a key feature that can be used to differentiate between competing models of CME initiation. We

also will be able to clarify the underlying physics linking the diverse *in situ* signatures seen in interplanetary ejecta, as well as their connection with CME properties.

As an illustration of how the imaging and *in situ* instruments on STEREO will be used to determine the physical structure of a CME as it progresses to 1 AU, consider the following observing sequence:

- a. Observe the signatures of CME onset on the disk with EUVI on both spacecraft.
- b. Observe a CME directed toward the trailing STEREO spacecraft (denoted STEREO-A, for clarity) with the COR2 and HI on the leading STEREO spacecraft (denoted STEREO-B). In addition, observe the approaching CME as a halo event with COR2 on STEREO-A.
- c. As the CME propagates toward STEREO-B, it is tracked with HI on STEREO-A. Any significant evolution in shape will be observed by both sets of imagers as the CME moves outward from the Sun.
- d. Track the CME-driven shock and particles to STEREO-B with the radio burst trackers on both spacecraft.
- e. Once the CME arrives at STEREO-B, sample the CME density, temperature, and magnetic field vector with the plasma analyzer and the magnetometer, and measure the 3D spectrum of energetic particles with the energetic particle detector.

This comprehensive set of measurements will be combined to give a definitive global picture of what a CME at 1 AU really looks like. Measurements by SECCHI and the other STEREO instruments will provide tremendous insights into the details of CME structure and evolution that are only alluded to by the fragments of information provided by present observations.

CMEs propagating outward into the solar wind can interact with corotating streams and their interaction regions (CIRs), interplanetary shocks, and transient flows. The interactions among these diverse phenomena is highly time-dependent, possibly changing qualitatively from day to day. Figure 1-10 shows an example from Behannon et al. (1991) illustrating the evolution over 4 days combining data from 4 well-separated spacecraft. The top panel shows an interplanetary event (ejecta-b) driving a shock S1 moving between two corotating streams and interacting with both streams. The

lower panel shows the situation just 4 days later, when the CIRs and ejecta-b had evolved. Between the two CIRs and behind the ejecta-b, two new ejecta (labeled c and d) were observed to interact with one another and with one of the CIRs. The data sets that resulted in Figure 1-10 are unique since the available solar-terrestrial data has been too sparse and uncoordinated to make such complementary measurements. STEREO will provide the first coordinated data set for studying the complex large-scale interactions in the heliosphere.

Solar energetic particle (SEP) events in the interplanetary medium sometimes accompany a CME. The accelerated particles are an important diagnostic of the CME evolution and its interaction with the ambient solar wind. The current, widely accepted paradigm is that impulsive and gradual SEP events are of different origin: impulsive events being flare associated and gradual events being associated with fast CMEs that drive interplanetary (IP) shocks (Cane et al., 1988; Kahler, 1992; Reames, 1997). Thus, observations from at least two vantage points are critical in understanding the mechanisms of acceleration and transport of energetic particles in three dimensions. The particle detector on the STEREO spacecraft trailing Earth will be magnetically well-connected to the source of an earth-directed CME, and thus will be well positioned to study prompt particles that are accelerated near the onset of the CME. The SECCHI COR2 and HI provide the remote sensing observations of line-of-sight integrals of the densities of heliospheric structures from the Sun to 1 AU. These observations will provide the necessary data to explore the physics of the interaction of the heliosphere with CMEs. The instrumental parameters to observe the interaction of CMEs with the heliosphere are shown in Table 1-4.

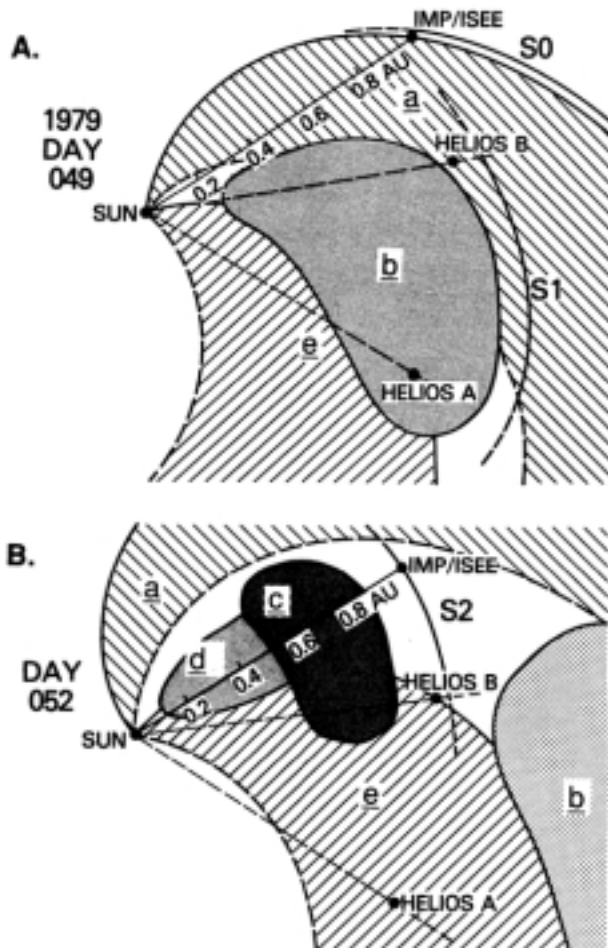


Figure 1-10. Interaction of CME with Solar Wind Flows

Table 1-4. Interaction of CMEs with Heliosphere: Instrumental Requirements

Inst.	FOV	Cadence	Resolution	Comment
COR2	15R _☉	3 per hour	30"	Observe passage of CME through the inner heliosphere
HI-1	85R _☉	1 per hour	1 arcmin	Observe interaction of the plasma cloud with the heliospheric structures
HI-2	1 AU	1 per 2 hours	10 arcmin	Observe interaction of the plasma cloud with Earth

1.2.5 Effects of CMEs on Space Weather.

Key Observational Questions

- Can the geo-effectiveness of CMEs be forecast?
- Can we predict if and when a CME will impact Earth?
- Can we predict if and when SEPs are generated?

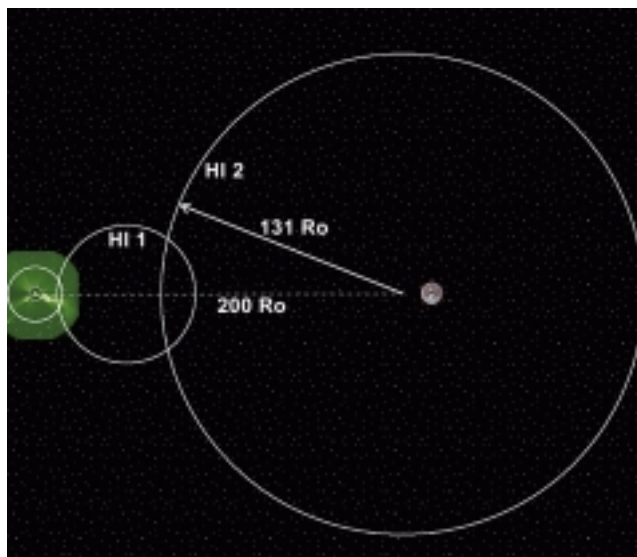


Figure 1-11. SECCHI FOV Centered on the Earth

As modern society becomes increasingly reliant on technologically advanced systems for many of its day-to-day functions, our ability to predict and respond to the impacts of space weather gains greater importance. The systems most susceptible to geomagnetic disturbances include the power grid and satellites, our reliance on which increases dramatically every year. The use of pagers and mobile phones has become almost ubiquitous. The global positioning system (GPS) is used heavily by the military, commercial airlines, and recreational boating, and is now being introduced into automobiles. As the use of these systems become more widespread, the effect of space weather disturbances impacts a wider array of people and human activities.

CMEs cause space weather disturbances, including the largest geomagnetic storms, in a number of ways. First, the magnetic fields in the CME reconnect with those of the terrestrial magnetosphere, producing strong induced fields and currents in the magnetosphere, the ionosphere, and the Earth's surface. Second, the impact of the CME compresses the Earth's day side magnetosphere down to lower altitudes, which can leave

high altitude geostationary satellites directly exposed to the solar wind and highly energetic particles. Third, the CME itself creates a shock wave that accelerates particles that can penetrate the Earth's magnetically shielded environment and occasionally reach the Earth's surface. An excellent example of this is shown in Figures 1-12 and 1-13 where a high speed CME is ejected from the west limb of the Sun. The energetic particles arrived at the orbit of SOHO and were detected as the 'snow storm' of cosmic ray hits on the LASCO CCD detector. These energetic particles pose a serious risk to astronauts, especially when outside their spacecraft.

An example of the apparent loss of a communications satellite and associated widespread loss of services due to a space weather disturbances has been described by Baker et al. (1998). They found that the combination of coronal mass ejections, solar flares, and high speed solar wind streams led to a prolonged period of geomagnetically disturbed conditions during which the Galaxy 4 communications satellite was subjected to an intense population of highly energetic, relativistic electrons.

Although recent strides have been made in our understanding of the relationship between CMEs and space weather, our current ability to forecast space weather disturbances caused by CMEs is still relatively poor. This applies to our ability to predict if and when a CME will impact the Earth as well as the magnitude of the anticipated impact (its geo-effectiveness). For the first time, the SECCHI suite of remote sensing instruments, together with the STEREO particle and fields instruments and the radio burst tracker, will provide the ability to predict accurately if and when a CME will impact the Earth. The LASCO and EIT observations from SOHO have demonstrated a first step in this prediction capability by reliably detecting halo CMEs—events that are directed along the Earth-Sun line and are visible as an expanding 'halo' around a coronagraph occulting disk. Halo CMEs were first identified with the NRL SOLWIND coronagraph (Howard et al., 1982) but only a handful were seen. With the increased sensitivity of the LASCO coronagraph, however, it is now possible to detect almost all of these events, while observations of the origin of the CME on the disk by EIT are used to determine whether the CME is headed toward or away from Earth. An analysis of halo CMEs (Brueckner et al., 1998) found that 8 of

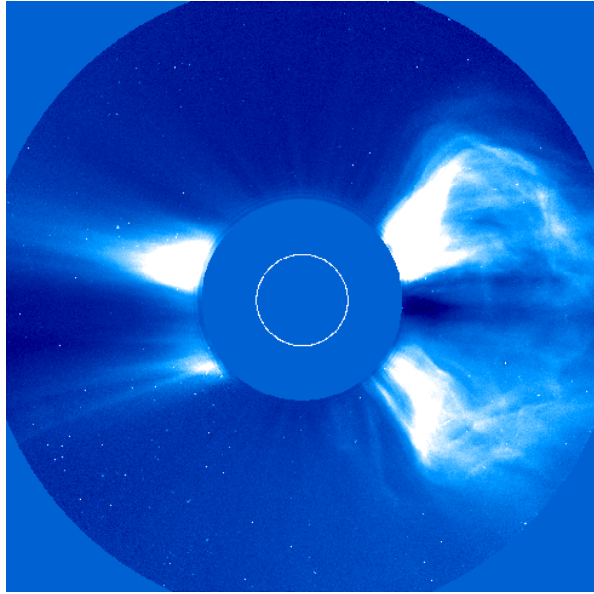


Figure 1-12. LASCO C2 Observations of a CME on 6 Nov 1997

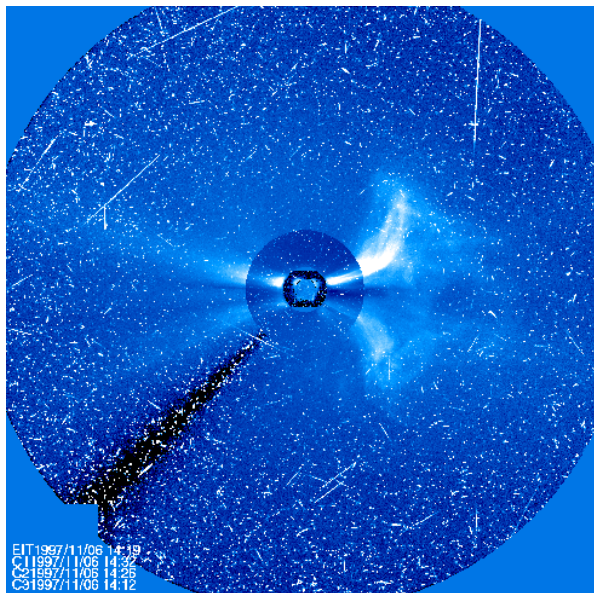


Figure 1-13. LASCO C2 Images Showing the "Snow Storm" of Energetic Particle Hits on the LASCO CCD Detector Caused by the 6 Nov 1997 CME

these events resulted in major geomagnetic storms ($K_p > 6$) roughly 80 hours after the CME was observed. Contrary to what one might expect, the 80 hour transit time appears to be independent of the CME velocity observed near the Sun. An important clue in understanding this seems to lie in recent observations by Sheeley et al. (1999). They have seen the deceleration of fast halo CMEs down to the solar wind speed, as seen in projection within the LASCO C3 field of view (FOV). We an-

ticipate significant improvements in our ability to predict the timing and impact of CME induced geomagnetic disturbances.

The eruption of Earth-directed CMEs will be detected by the EUVI, COR1, and COR2 experiments. Early in the mission, when the STEREO spacecraft are near the orbit of Earth, COR2 will record halo CMEs produced by front-side sources detected with EUVI. As the separation of the STEREO spacecraft increases, the different vantage points will allow us to determine the velocity vector of the CME, as well as the material that will directly impact Earth. The velocity vector will be determined by means of triangulation techniques involving simultaneous stereo image pairs. In cases where simultaneous image pairs will be obtained with EUVI, COR1, COR2, and HI, the velocity vector should reveal the acceleration of slow CMEs and the deceleration of fast CMEs, thus accounting for the general 80 hour transit time from the Sun. A real advance in our ability to predict the arrival of CMEs at Earth will be provided by the HI, which will track CMEs throughout their trajectory to Earth. This is an important component of our space weather prediction capability. Near solar minimum, when STEREO will be in operation, even moderate strength CMEs can have significant geomagnetic effects. Consequently, just the simple ability to predict the arrival at Earth of a CME will be important.

The next step in advancing our understanding of space weather lies in predicting the geo-effectiveness of CMEs, which is strongly governed by the southward component of its magnetic field, B_z (Gonzalez et al., 1994). Strong B_z can be created in several ways, from a strong internal B_z in the plasma configuration ejected from the Sun, by shock compression of the field in fast CMEs, and by the interaction of the CME with strong fields in the heliospheric plasma sheet (HPS). In all cases, the complete diagnostic capabilities of the SECCHI investigation will be needed to disentangle the various components involved in the complex interaction of the CME with the magnetosphere.

One way to predict the direction (north vs. south) of the magnetic field of a CME that impacts the Earth is based on the conservation of magnetic helicity in MHD systems (Taylor, 1974). If we assume that the CME is produced by the reconnection of the magnetic field lines in an arcade overlying the neutral line, the helicity of this configura-

tion will be preserved during the reconnection process. By inferring the helicity of the magnetic arcade/prominence that produces the CME, then we can predict the helicity, and the polarity of B_z , in the CME that arrives at Earth. This will be done with the SECCHI instruments as follows:

- Determine the location of the eruption from EUVI images.
- Use VMAG to measure the photospheric magnetic field on both sides of the eruption.
- Determine whether the helicity is left- or right-handed from the orientation of the coronal field lines seen in EUVI coronal lines.
- Use the HI observations to determine whether the impact with Earth will be head-on or at a glancing angle.

The use of helicity conservation is shown graphically in Figure 1-14. Bothmer and Rust (1997) found that this technique was successful in predicting the initial B_z in 34 out of 37 magnetic clouds observed by *Helios*.

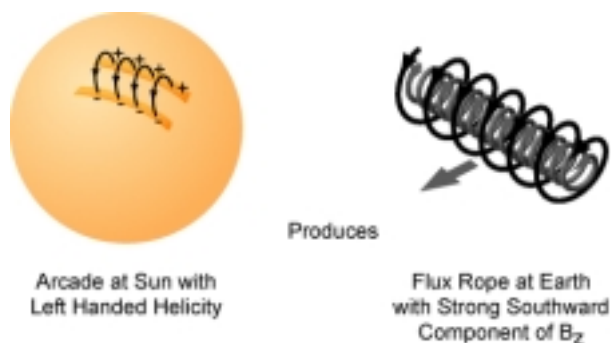


Figure 1-14. A magnetic arcade with left-handed helicity at the Sun the produces a flux rope at Earth with a strong southward component of B_z .

1.2.6 Analysis Techniques. With proper 3D analysis tools, the unprecedented sets of SECCHI data will lead to breakthroughs in our understanding of the physics of CMEs and other related phenomena. The 3D reconstruction tools and 3D plasma/magnetic field simulations are an integral to the success of SECCHI science investigation.

□ **3D Reconstruction Tools:** To date, our entire perception of the solar corona is derived from 2D images from a single viewpoint. A stereo-like reconstruction has been attempted for Skylab, *Yohkoh/SXT*, and SOHO/EIT images in which solar rotation provides the stereo separation (e.g., Berton and Sakurai, 1985). But these attempts had only limited success, due primarily to highly vari-

able coronal structures. For the first time, STEREO will provide a second vantage point from which 3D information can be derived. A viable reconstruction technique is triangulation on identifiable features observed by viewpoints (tiepoints). The technique has been successfully tested on simulated stereo X-ray data (Gary et al., 1997) and on rotational stereo EUV data (Liewer et al., 1997). The accuracy of the triangulation technique depends in part on resolution and pointing and in part on the stereo angle.

For the first time, the SECCHI instruments, especially HI, will track CMEs from the Sun to the Earth. Triangulation techniques are capable of determining the velocity vector for diffuse objects such as CMEs. We have used a synthetic stereo coronagraph image pair created from a 3D flux-rope model of a CME to test this. This stereo image pair is shown in the top two panels of Figure 1-15. By visually locating a series of tie points in both images, it has been possible to reconstruct the 3D location of the tie points. These are shown at the bottom of Figure 1-15. On the left, the reconstructed CME front is viewed from the side, and on the right, the CME front is viewed head on. In summary, triangulation techniques, especially when combined with tomographic reconstructions of CME observations, should provide an accurate calculation of the CME velocity vector.

SECCHI will observe a propagating CME from the two spacecraft as a sequence of image pairs. From these data, tomographic techniques will be used to determine the 3D structure of a CME and its evolution. Solar tomography is at an early stage of development. Panasyuk (1999) and Zidowitz (1999) have demonstrated its use in reconstruction of 3D models of the quiet corona from images obtained over a solar rotation. Zidowitz has found considerable longitudinal variations in the streamer structures. Similar techniques have been explored by Davila (1994). Jackson et al. (1998) used IPS data together with a model to derive the heliospheric density structure. Additional constraints often aid the reconstruction process. For example, Jackson and Froehling (1995) assumed a constant radial velocity in their reconstruction of a CME observed with SOLWIND and *Helios*. For SECCHI, the degree of polarization measured in COR1 and COR2 provides an additional constraint that must be folded into tomography techniques.

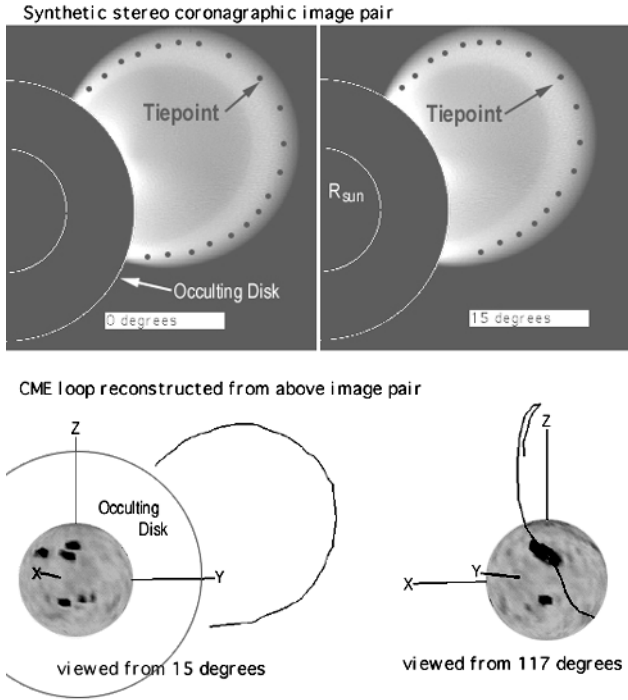


Figure 1-15.

Top, synthetic coronagraph stereo image pairs of a CME with the locations of tie points.
 Bottom, the outline of the CME reconstructed from the tiepoints viewed at the limb (15 degrees) and head on (117 degrees).

❑ **3D Model Development:** SECCHI numerical models will play an essential role in the success of the whole STEREO mission, and the results will be treated as data products to be distributed via the internet. There are two principal aims of the modeling efforts:

- a. Modeling the large-scale quasistatic plasma parameters provides the input necessary to determine fully the field's structure and dynamics in the corona and heliosphere.
- b. Applying sophisticated numerical models to quantify the relationships between phenomena observed remotely by imaging of the Sun and those measured in situ at 1 AU.

We have assembled a uniquely qualified team of modelers. The Co-I groups at NRL and SAIC are world leaders in large-scale coronal simulations and the SECCHI program will benefit immensely from the substantial investments in code development that these teams have already made.

❑ The SAIC group will develop WIND3D, a model designed to determine the large-scale, quasi-steady, 3D plasma and magnetic structure of the solar wind. This model will use the semi-implicit numerical methods pioneered by SAIC for long-

Table 1-5. SECCHI Instrument Cadence & Data Rate

Inst.	Format	No. of Images	Cadence	Fraction Transmitted	Compress Factor	Data Rate (tb/s)
Nominal (End of Life) Telemetry						
VMAG	1024 ²	4	30 min.	0.785	4	6.4
EUVI	1024 ²	2	2.5 min.	0.785	10	15.3
	2048 ²	2	30 min.	0.785	10	5.1
COR1	1024 ²	3	8 min.	0.75	10	6.9
COR2	2048 ²	3	30 min.	0.985	10	9.6
HI-1	1024 ²	1	60 min.	1	2	2.0
HI-2	1024 ²	1	120 min.	1	2	1.0
Total						46 kb/s

time integrations of slowly varying MHD systems (Linker and Mikic, 1994).

❑ The NRL group will develop TRANS3D, a code designed to model transient events, particularly CMEs, initiated near the Sun and propagating to the Earth. TRANS3D will be a 3D spherical code employing a fully adaptive mesh, and will build on the numerical technology for handling MHD shocks, current sheets, and other discontinuities that was pioneered at NRL (Antiochos and collaborators).

❑ The WIND3D and TRANS3D models will require an intensive development and testing effort to interface them with each other and with the SECCHI data. This work must begin in phase B to have them ready for use by the STEREO launch.

1.3 Observational Requirements.

1.3.1 SECCHI Instrument Cadence. Limited telemetry resources require trade-offs between image cadence, degree of on-board image compression, and wavelength coverage (for the EUVI). Pixels may be binned on chip to reduce the readout time or may be summed within the computer to increase the dynamic range. For example, an image can be resized to 512 x 512 by performing 4x4 pixel summing within the SECCHI computer. Table 1-5 shows a possible observing plan. It reflects the nominal telemetry rate expected late in the mission. Substantially higher rates may be available earlier in the mission. We can vary the rate to permit the PIETRO experiment to occasionally enter an observing program requiring more telemetry.

1.3.2 Traceability Matrix. Table 1-6 summarizes the main scientific goals of the instrument and

Table 1-6. Science and Instrumentation Traceability Matrix

Science Objectives	Physical Property to be Observed	STEREO Viewpoint	Instruments									
		Required	SECCHI					Beneficial Contributions				
			VMAG	EUVI	COR1	COR2	HI	Waves	Particles & Plasma	models	Solar B	Ground Based
What is the 3D structure of magnetic field, coronal loops, helmet streamers?	Magnetic field and density structure of the corona	Yes	√	√	√	√	√	√	√	√	√	√
What are the 3D properties of CMEs?	Evolution of 3D density and magnetic field structure of CME with time	Yes		√	√	√	√	√	√	√		√
What is the timing of physical processes involved in CME Initiation?	Identify coronal structures, EUV waves, possible global interactions	Yes	√	√	√	√			√	√	√	√
	Identify absolute timing of CME onset and energetic processes	No		√	√	√		√	√			√
What are the critical forces controlling propagation of CMEs in the corona and interplanetary medium?	Evolution of 3D density, magnetic fields	Yes	√	√	√	√	√			√	√	√
	Speed, acceleration and deceleration of CMEs	Yes		√	√	√	√			√		√
	Interaction of CME with corona and IPM, formation of shock, sweep-up of ambient material	Yes				√	√	√	√	√		√
What CME properties are significant for space weather predictions?	Magnetic and density topology	Yes	√	√	√	√	√	√	√	√		
	Speed and direction of CME	Yes		√	√	√	√	√	√	√		

which instruments will contribute to satisfying those goals.

1.4 Instrument Overview. The SECCHI instrument suite contains a complete set of instrumentation to explore the inner Heliosphere from the photosphere to the earth. This set of instrumentation will maximize the scientific opportunity afforded by the continuously changing vantage points of the two STEREO spacecraft by obtaining a comprehensive set of observations at the various viewing angles. It will obtain remote sensing observations of the photospheric magnetic field, full sun EUV images of the chromosphere and inner corona as well as white light images from 1.1 to 332 solar radii. To accomplish the required observations, we propose to build six relatively simple, specialized optical trains to address each observational task.

Our instrument suite consists of two optical packages, a Sun-Centered Imaging Package (SCIP) and the HI package. Each of these two individual packages consists of a spar-type common optical support structure for its telescopes, under the control of common electronics.

□ The SCIP contains four compact telescopes to view the solar disk and solar corona held in precise coalignment through an innovative structural de-

sign. Two coronagraphs are used to optimize stray light rejection over the different ranges of height in the solar atmosphere. An EUV imager is used to establish the emission line corona over the disk and low corona as well as to observe the He II transition region network structure and prominences. A magnetograph is attached to the required fine guide telescope to extend the latitudinal coverage of the photospheric field with little additional consumption of resources.

□ The HI package contains two simple lens telescopes to directly view the sun earth line. These two telescopes are sheltered within a protective baffle structure to obtain the necessary rejection of bright objects outside the field, including the solar disk, and spacecraft glints.

The individual characteristics of the SECCHI telescopes and responsible institutions are given in Table 1-7. As described in the following sections, the telescopes use well-characterized designs that have a proven track record. The telescopes will be constructed by experienced teams under the leadership of a senior SECCHI co-investigator at the various participating institutions. The division of labor and clear lines of responsibility greatly simplify the task of managing the SECCHI development effort. Finally, economy and reliability are

enhanced by employment throughout of standardized subsystem designs with significant flight heritage. The advanced SECCHI instrument suite satisfies all the requirements of the STEREO program for the SCIP and HI instrumentation within technical and programmatic resources.

1.4.1 Coronagraphic Investigation. The scientific goal of exploring the white light corona from 1.1 to 332 solar radii requires innovation in the design of instrumentation, for this has never before been accomplished. The fundamental difficulty of obtaining the necessary rejection of the photospheric disk is compounded by the enormous gradient in coronal brightness (Figure 1-16). The surface brightness (total K+F) varies by seven orders of magnitude across this scene; further, the coronal mass ejection signals in interplanetary space are expected to be ~ 240 times fainter than the zodiacal light cloud. Thus, an instrument dynamic range of $>2 \times 10^9$ is needed.

Fortunately, while the observational difficulties vary strongly with radial distance from the sun, the requirements also vary with radial distance. For example, high spatial resolution, of critical importance at the disk and in the inner corona, is less necessary at greater elongations, where the scale lengths are much larger. Also, where low levels of stray light are required for recording dim coronal and CME signals in interplanetary space, these can be achieved by moving the entrance aperture of the telescope further into the shadow of the external occulter and sacrificing the innermost FOV.

The four fields of view of the white light instrumentation are shown in Figure 1-16. The two coronagraphs provide coverage of the corona from 1.1-4 and 2-15 solar radii respectively. The COR1 coronagraph is internally occulted. This allows high spatial resolution observations of the corona to be obtained below 2 solar radii albeit at the cost of a considerably increased stray light level. The stray light performance is expected to be similar to that achieved with the successful C1 coronagraph on SOHO. The central difference from the SOHO instrument is that the COR1 instrument is optimized for exploring the white light corona with polarization techniques instead of obtaining detailed intensity line profiles of the emission line corona. The COR2 instrument is a modified version of the existing wide field coronagraph on SOHO and is externally occulted. The external occultation provides superb stray light rejection but re-

stricts the inner field limit to ~ 2 solar radii. Both coronagraphs will obtain brightness and polarized brightness images of the white light corona.

The HI package will concentrate on producing high quality images of the Heliosphere along the sun-earth line as shown in Figure 1-16. Near solar minimum, activity in the outer solar corona is concentrated at the equatorial streamer belt. The C3 coronagraph observations show that CMEs are directed along the equatorial current sheet with a full angle spread of ~ 82 degrees. The FOV of the HI-1 and HI-2 are optimized to obtain high quality observations of this critical region. Designing the two telescopes for these two fields of view as opposed to a single FOV of a hemisphere minimizes restrictions on spacecraft protrusions and reduces dynamic range requirements for each telescope. The resulting instrument is greatly simplified and will be designed, constructed and tested with straightforward and well known coronagraphic and optical techniques. This simplification greatly reduces the technical risk and complexity associated with the HI package.

The essential signal levels of the white light corona are given in Figure 1-16. The fundamental observational requirement is to obtain the coronagraph images with sufficient photometric precision to discriminate the electron scattered corona from the background signals of F-corona, instrumental stray light and stellar/planetary sources. The single most stringent detection requirement inherent in the STEREO science objectives is the detection of the coronal mass ejections and the derivation of their properties (speed, direction, density and internal structure). The SECCHI white light coronal instrumentation has been particularly optimized to observe coronal mass ejections throughout its FOV with a reasonable cadence. Figure 1-16 presents a comparison of the one sigma detection limit for the coronagraphs with nominal CME signal levels. As shown on the graphs, the SECCHI instrumentation will readily detect coronal mass ejections over its entire FOV. In the outer fields of the coronagraphs, the effective spatial resolution will be reduced but we still expect to readily identify the location of CME fronts and internal structures and their intensities.

1.4.2 Identification of the K-corona and CMEs in SECCHI Observations. Having obtained images with the necessary precision, the essential analysis problem is to distinguish the

Table 1-7

	COR1	COR2	HI	EUVI	VMAG
Instrument Type	Internally Occulted Lyot Coronagraph	Externally Occulted Lyot Coronagraph	Externally Occulted Coronagraph	EUV Narrow- Band-pass Cassegrain Telescope	Solid Fabry-Perot Double Etalon Magnetograph
Lead Institute	NASA/GSFC	NRL	Univ. of Birmingham	LMSAL	LMSAL
Related Projects	Mauna-Loa Mk-III and SPARTAN 201 Coronagraphs	LASCO and SOL-WIND Coronagraphs	STP SMEI, LASCO Consortium	TRACE, GOES-N SXI, YOHKOH SXT	Trace Guider MDI, Solar-B Polarimeters, and Skylab H-alpha Imager
Observable	K-Corona and CMEs	K-Corona, F-Corona and CMEs	K-Corona, F-Corona and CMEs	Emission Line (EUV) Corona & Upper Chromosphere	Photospheric Vector Magnetic Field
Field of View	1.1 - 4 R _⊙	2 - 15 R _⊙	12 to >215 R _⊙ HI-1: 12-84 R _⊙ HI-2: 66-318 R _⊙	0 to 1.5 R _⊙	0 to 1 R _⊙
Spatial Scale	7.5" pixels	15" pixel	HI-1: 35.2" pixels HI-2: 120" pixels	1.4" pixels	2.1" pixels
Focal Plane Array	1024 x 1024 (2k x 2k array summed 2x2)	2048 x 2048	1024 x 1024 (2k x 2k array summed 2x2)	2048 x 2048	1024 x 1024 (2k x 2k array summed 2x2)
Bandpass	650-750 nm	450-750 nm	450-750 nm	He II 30.4 nm Fe IX 17.1 nm Fe XII 19.5 nm Fe XIV 21.1 nm	630nm
Exposure Times	1 to 4 sec 3 required for pB	3 sec 3 required for pB	HI-1: 12 sec HI-2: 60 sec Exposures >8 required	Fe IX: 3 sec Fe XII: 5 sec Fe XIV: 7 sec He II: 10 sec	50 ms per exposure (8 required)
Maximum Cadence	15 sec	36 sec	HI-1: 1 min HI-2: 8 min	11 sec at <i>full resolution</i> in Fe IX (4.75 sec at <i>half resolution</i>)	33 sec
Synoptic Cadence	8 min	30 min	HI-1: 1 hour HI-2: 2 hours	20 min <i>full resolution</i> and 2.5 min <i>half resolution</i>	30 min
Critical Alignment Tolerance	125 micron (separation of lens elements)	1 arcmin alignment of ext. & int. occulters	0.5 mm (Baffle planarity)	10 micron (primary to secondary)	200 micron (separation of lens elements)
Absolute Pointing Required	10 arcsec occulter positioning	45 arcsec occulter positioning	30 arcmin	3 arcmin FOV overlap	2 arcmin FOV overlap & linear guider range
Pointing Stability Required	1.5 arcsec over pB sequence (11 sec)	1.5 arcsec over pB sequence (25 sec)	0.5 arcmin over HI-2 sequence (1hr)	1.5 arcsec over 3 exposures (39 sec)	1.5 arcsec over 33 sec
Long Term Pointing Required	5 arcsec over a month to obtain background subtraction model (F-corona + Straylight) for total B determination		5.0 arcmin to obtain background model	N/A	N/A
Mechanism Count	1 shutter 1 rotating wave plate	1 shutter 1 rotating wave plate	1 shutter	1 bandpass shutter 1 filter wheel 1 CCD shutter	1 shutter 1 rotating wave plate
Optical Bench	SCIP (Coronagraph Half)	SCIP (Coronagraph Half)	HI Structure	SCIP (Disk Imager Half)	SCIP (Disk Imager Half)
Thermal Control	SCIP System	SCIP System	HI System	SCIP System	SCIP System & F-P Oven
Aperture	36mm	30.5 mm	HI-1 16 mm HI-2 21mm	90mm	40mm
EFL	f/20	f/6	HI-1 f/5 HI-2 f/2.8 to f/4.8 (center to FOV limit)	f/22.2	f/64
Straylight/Disk Light Rejection	10 ⁻⁶ B _⊙	10 ⁻¹¹ B _⊙	HI-1 10 ⁻¹³ HI-2 10 ⁻¹⁴ B _⊙	10 ⁻¹² ratio of visible/EUV	Isolate 630nm line to 10nm FWHM 0.01 nm
CCD	EEV 42-40, 2k x 2k, 13.5 μm pixels, backside illuminated, AR coated (except EUVI), >100k e ⁻ full well				
Camera	Common electronics, 500 kHz readout rate, 14 bit/pixel digitization				

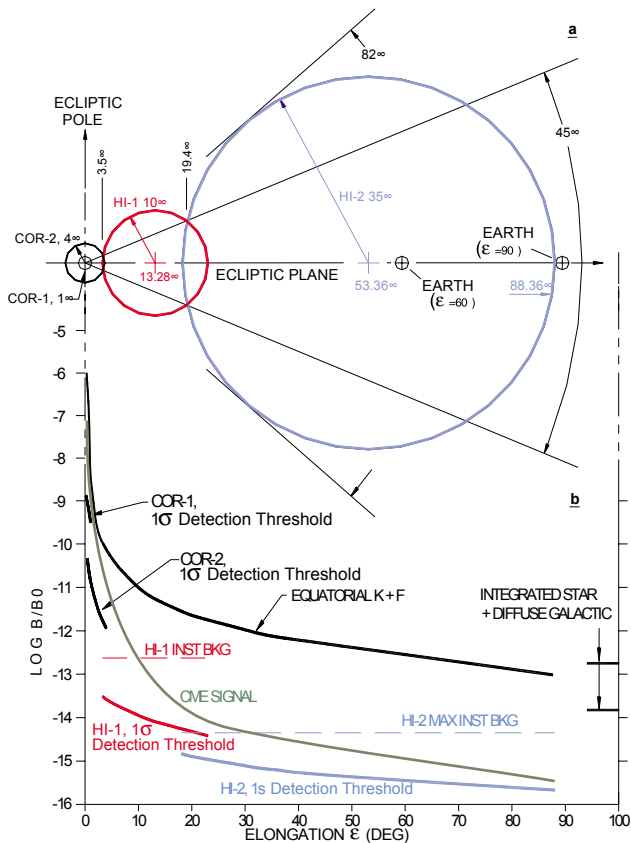
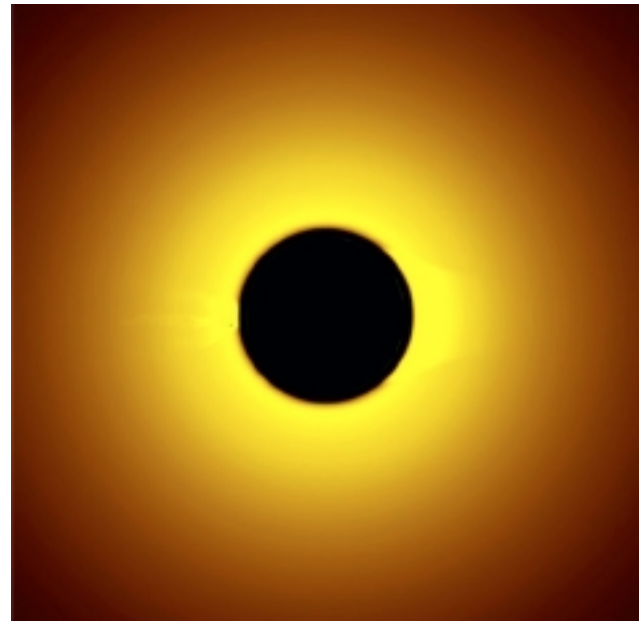
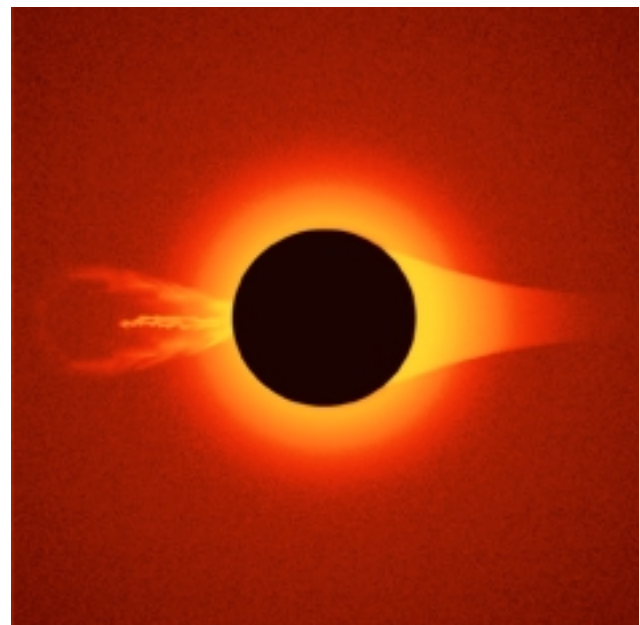


Figure 1-16. HI-1 (red) and HI-2 (blue) fields of view strongly time varying signal of the K-corona with its streamers, plumes and transient structures from the relative bright and static background comprised of the F-corona, planetary/stellar sources and instrumental stray light. For the SECCHI instrumentation, we will accomplish this with two classic techniques. These two techniques have been successfully used to analyze coronagraph images for the past three decades.

□ **Polarization Analysis:** Polarization analysis of the COR1 and COR2 images will be used to separate the K-corona from instrumental scatter and the F-corona. In the low corona, the F-corona and instrumental stray light is unpolarized while the K-corona is strongly polarized. Thus, polarization analysis will separate the K-corona signal from the instrumental stray light and F-corona. In contrast to prior missions, the coronagraphs are specifically designed to obtain the polarized brightness images with a cadence and SNR compatible with detecting coronal mass ejections. An example of this technique on a model CME using the Mauna Loa Mk III coronagraph stray light conditions is presented in Figure 1-17.



(A) Raw Image



(B) Recovered Polarized Image

Figure 1-17. Raw and Recovered Polarized Images

The polarization analysis will be obtained by the same technique in both COR1 and COR2. A rotatable half-wave plate similar to the Precision Achromatic Retarder from Meadowlark and a fixed polarizer of the type Polaroid HN22 (or similar to Polarcor) is integrated into the optical path. Images are taken in succession through this system with the half-wave plate at -30, 0 and +30 degree positions respectively (giving polarization angles at -60, 0, and +60 degrees). Polarization (%p), po-

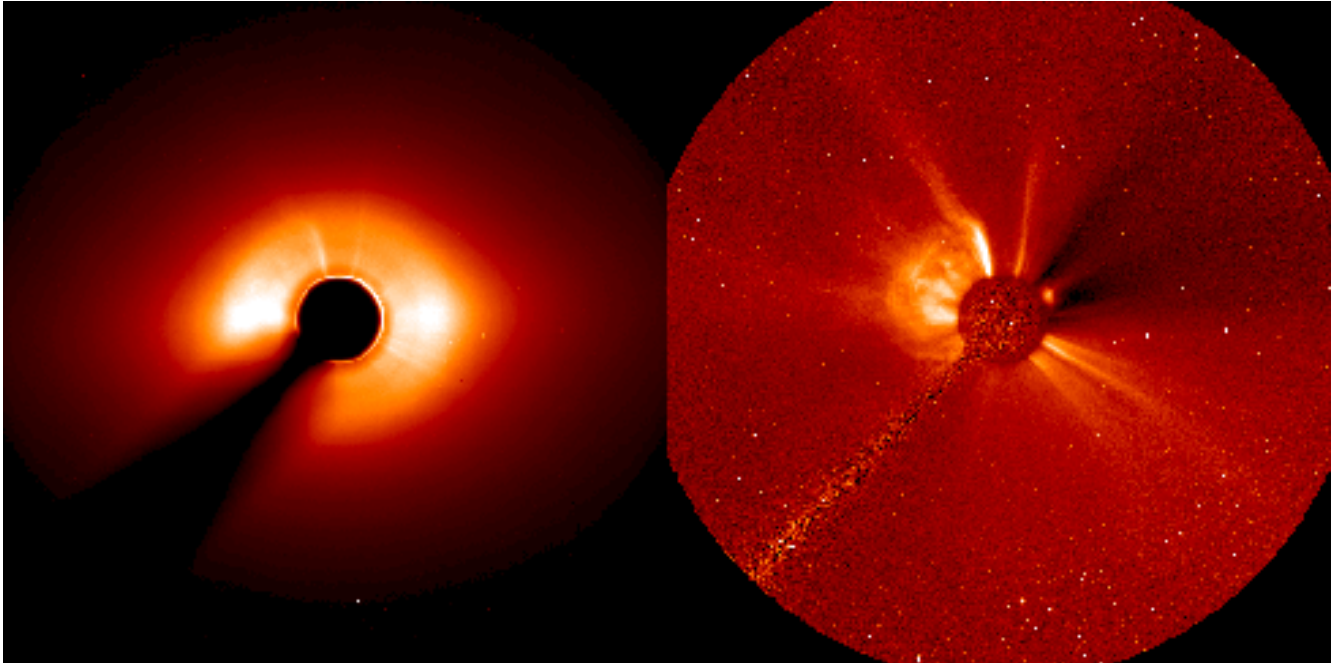


Figure 1-18. Stray/Zodiacal Light Model Subtraction

LASCO/C3 Coronal Image Taken on 20 June 1999: The left panel shows the typical football shaped distribution of the zodiacal light (F-corona) that overlies the dimmer K-corona at moderate and long elongations from the Sun. In the right panel, the zodiacal light and the stray light have been removed to show clearly the background stars, coronal streamers and a CME in progress in the north east.

larization brightness (pB), and brightness (B) are determined from the three images with standard algorithms. The 100 nm bandpass of the COR1 is more limited than the bandpass of COR2, so the design of the half-wave plate is somewhat easier. However, Medowlark Inc. has expressed an interest and confidence in fabricating an half-wave plate for the full 450-750 nm bandpass.

□ *Background Model:* Another technique has been to create an overall background model which consists of the static K-corona, the F-corona, and instrument stray light from the instrument itself. We expect to create this model by calculating the daily medians of the images for the four weeks surrounding the particular day of interest and determining the minimum of these daily median images. The STEREO spacecraft orbit radius will have significant variation. This effect will be de-trended from the daily median images if necessary utilizing existing procedures developed for analysis of the LASCO data. These de-trended daily median images will then be used to calculate the background images. The processing of the HI images will also include an optional removal of the stellar images with a combination of a synthetic star map and the information present in the images. The background subtraction technique will be

applied to all the images from the SECCHI white light coronal instrumentation to derive the time-varying K-corona component; in particular, these images will be used to address the derive the intensity of the total Thomson scattered radiation in CMEs, plumes and evolving streamers. An example of this technique applied to a LASCO/C3 image is presented in Figure 1-18. Note that, although the images in COR1 and COR2 are taken through a polarizer, since the retarder mechanism can be rotated to any angle, a total B image can be summed onboard from just two exposures at 0 and 90 degrees.

□ *Comparison of Technique:* The two techniques will result in polarized and unpolarized intensity images of the K-corona. Both techniques represent a weighted measure of the electron density along the line of sight. The relative weighting of each electron along the line of sight is quite different between the two techniques. The polarized brightness observations have sensitivity to within ± 50 degrees from the plane of the sky while the total brightness observations are sensitive to ± 75 degrees from the plane of the sky. For example, at 50 degrees from the plane of the sky, the relative polarization brightness has decreased 90% while the relative total brightness has decreased only 40%

FOV scanning system analogous to the 1° - 3° full field design employed on HELIOS (Leinert and Klüppelberg, 1974). The optical system itself, or a folding mirror, could be used for scanning. This concept met the 10^{-14} B/B_\odot rejection requirement at high elongation but was opto-mechanically complex, had low throughput (light gathering power \times dwell time at any given field position) and the onboard full field image accumulation and registration task too was computer intensive. The third design concept attempted to solve the deficiencies encountered in the first two by using a stationary, side looking, and nearly hemispheric full field angle lens surrounded by a relatively planar baffle system (e.g., Buffington, 1998). This concept resulted in a low light gathering power (<1 mm diameter usable aperture for any given field position) due to the extremely wide field angle in combination with the physical size of the available CCD. Furthermore, part of the domed convex lens projected well up into the poor light rejection zone of the planar baffle system unless it was made excessively large. This study indicated that achieving a near sun view angle and a night sky instrumental background at large elongation with a single lens would be difficult, and possibly catastrophic for the night sky portion of the field.

The first three concept studies indicated that the most appropriate instrumentation for the CME detection task changes substantially with elongation. Whereas the relatively bright and narrow field required at small elongation suggested an externally occulted coronagraph, the low night sky brightness, background noise limited detection, and wide field required at high elongation suggested a heavily baffled, high light gathering power all-sky telescope. The fourth concept studied, the proposed HI, accommodates these disparate requirements with two specialized optical systems (HI-1 & HI-2) in a single progressively baffled configuration (Figure 1-19).

□ *Description:* The HI-1 system uses a five vane forward linear baffle system and matching linear internal occulter, a 20° full field angle lens, and a 2048×2048 pixel format CCD. It is similar to a coronagraph. A small baffle over the lens protects it from earthshine. Fresnel diffraction calculations (Born & Wolf, 1980), with forward baffle vane heights optimized for the HI-1, show it will achieve an instrumental background $\leq 3 \times 10^{-13}$ B/B_\odot at $E = 3.28^\circ$. This is substantially below the

natural K+F corona background and a factor of 10 better than the $<10^{-12}$ B/B_\odot (Brueckner et al., 1995) achieved on SOHO/LASCO/C3 (due to the 12.3R rather than 3.8R inner field cutoff).

The HI-2 optic is set much more deeply within the HI-1 forward baffle system shadow at a large diffraction angle of 16.5° (lens top edge), where the forward baffle diffraction calculation result is 2.3×10^{-18} B/B_\odot . This system is akin to a wide-angle night sky camera. In order to minimize solar stray light rejection risk, an additional HI-2 optimized forward baffle system is used along with a matching internal occulter. There is also a separate rear baffle system to block light from the HI-1 entrance aperture and early mission earthshine, an earthshine rejection mirror, a moderately wide-angle and large aperture (Mori type) fisheye lens, and a 2048×2048 pixel format CCD. The instrumental background for HI-2 is dominated by veiling glare from earthshine diffracted at its entrance aperture stop rather than forward baffle diffracted solar light. The maximum instrumental background is 5×10^{-15} B/B_\odot for a S/C-earth lead (lag) angle of 2° and diminishes approximately with the inverse square of the S/C-earth distance, since earth's phase change is relatively small.

By using the second entrance aperture at a greater diffraction angle, additional baffling and a moderate (70°) wide angle lens with greater light gathering power than a hemispherical field angle lens; we mitigate stray light rejection risk, improve threshold background noise limited signal detection at large elongation, especially along the critical sun-earth line, while reducing overall planar baffle system size. The superior diffraction angle afforded the night sky portion of the field in this design is important, since solar stray light rejection is the paramount risk. This approach to risk mitigation is driven by the fact that empirically determined baffle diffraction performance has not been established below about 10^{-8} B/B_\odot for these wide angle type Fresnel diffraction baffle systems (Buffington et al., 1996; Romoli et al.).

□ *Operation:* The HI uses a single 30° stepper motor and wheel shutter system. Wheel design allows both HI-1 and HI-2 to operate without affecting the state of the other. Individual HI-1 exposure times are approximately 12 sec at $\leq 50\%$ saturation and HI-2 ~ 1 min at $\leq 40\%$ saturation. Only <10 th magnitude stars ($\sim 0.6/\text{deg}^2$) will saturate the CCD

and anti-blooming will contain them. Individual exposures are cosmic ray scrubbed by a running comparison of three consecutive images (summed subsets of images for HI-1), optionally binned, and accumulated (32 bit) in the main computer memory for an effective exposure time on the order of 1/2- to 1-hour. Calculations indicate that stars, cosmic rays and photon noise can be distinguished in the scrub. While the lowest level cosmic ray charges are not distinguishable from photon noise at 3σ with the planned assembly language routine, their charge and number density is low ($\sim 1/\text{pixel}/2.8$ hr.) enough that their residual contribution is below photon noise in the final, summed, image. The shutter wheel includes a flat field calibration diffuser position, which can be back-illuminated by the sun with a spacecraft yaw maneuver. Since each lens views dark space, each has a heater to prevent condensate contamination.

□ *Performance:* A high quality image is important for the stereographic reconstruction process. Paired images used in reconstruction must be radiometrically consistent and have high signal to noise ratios. Radiometric consistency can be satisfied with a stable CCD camera, a repeatable shutter, a good preflight spectral responsivity calibration and a lens design with minimal aberrations.

Both photon statistics and CME proper motion affect image spatial resolution. The photon statistical resolution can be estimated with a SNR metric (Rose, 1948). The lower curves in Figure 1-16 show the single pixel 1s precision brightness for photons accumulated during a 1-hr. exposure. It can be seen that the ratio of the CME signal to the rms photon noise ranges from about 10σ down to 2σ over the full elongation range. CME proper motion is $\sim 1^\circ/53$ min, so a 48 min exposure with a 32×32 pixel binned superpixel resolution element ($\sim 1^\circ$) matching CME travel would have a SNR ranging from about 286σ down to 57σ . A SNR ~ 5 per spatial resolution element is required for threshold detection of a simple, known *a-priori*, target on a flat background (Rose, 1948, Barrett, 1990) and substantially higher photon statistics ($\geq 30\sigma$) are required for more complex images and stereographic reconstruction (Rose, 1953). Since parts of some CMEs will not be seen by both S/C, the SNR margin is reasonable.

b. Outer Coronagraph. The successful LASCO/C3 coronagraph on SOHO is used as the basis for the COR2. We first attempted to ex-

tend the LASCO/C2 design, but it far exceeded the STEREO mass constraint. For COR2, we have therefore reduced the outer limit of the more compact C3 design from 30 to $15 R_\odot$, and reduced the inner limit from 3.7 to $2.0 R_\odot$. The span in coronal brightness is about the same as that covered in C3 (200x). For LASCO/C2 an inner limit of $2 R_\odot$ produced a stray light level of about 10^{-11} . In the hybrid design that is COR2, we are confident that the range of $15 R_\odot$ is easily achievable in a single instrument. Thus, the COR2 concept presented here is a mature design, easily achievable, and which meets all of the science requirements.

□ *Optical Description:* The COR2 design is a traditional externally occulted Lyot coronagraph extending from the inner limit at $2 R_\odot$ to the outer limit at $15 R_\odot$. A coronagraph is a relatively simple telescope with the added complexity of extreme stray light rejection techniques. Figure 1-20 shows the concept of stray light suppression in a Lyot coronagraph. Photospheric light is blocked by the external occulters (here a 3 disk system), but diffraction occurs at the edges of the circular disks. Each disk captures the diffracted light from the previous disk, so that the photospheric light is significantly reduced in the plane of the entrance aperture, A1. For COR2, we calculate the attenuation to be 10^{-5} for a triple disk occulter with 50 mm spacing between the disks and 400 mm from the last disk to A1.

The singlet objective, O1, is made of super-polished, low scattering glass (BK7). O1 images the last disk in D1 onto the internal occulter, D2, which is just slightly larger than the image of D1. This captures the last diffracted light around the D1. Another significant component to achieving stray light reduction are the A1 and A3 apertures. The A1 aperture is completely shadowed by D1, but significant diffraction still occurs at the edge of A1. This light is imaged onto the A3 stop (Lyot stop) by O2, where it is captured by the slightly undersized A3 stop. A third stray light component is captured by the Lyot spot, which is a small black disk just before the relay lens, O3. The Lyot spot captures any ghosts generated by internal reflections within the O1 objective. The total stray light rejection is computed to be about 10^{-11} which is well below the coronal brightness. Figure 1-20 illustrates the COR2 optical system. It operates at $f/6$, which is less than the $f/9.3$ LASCO/C3. This faster system together with the brighter corona in

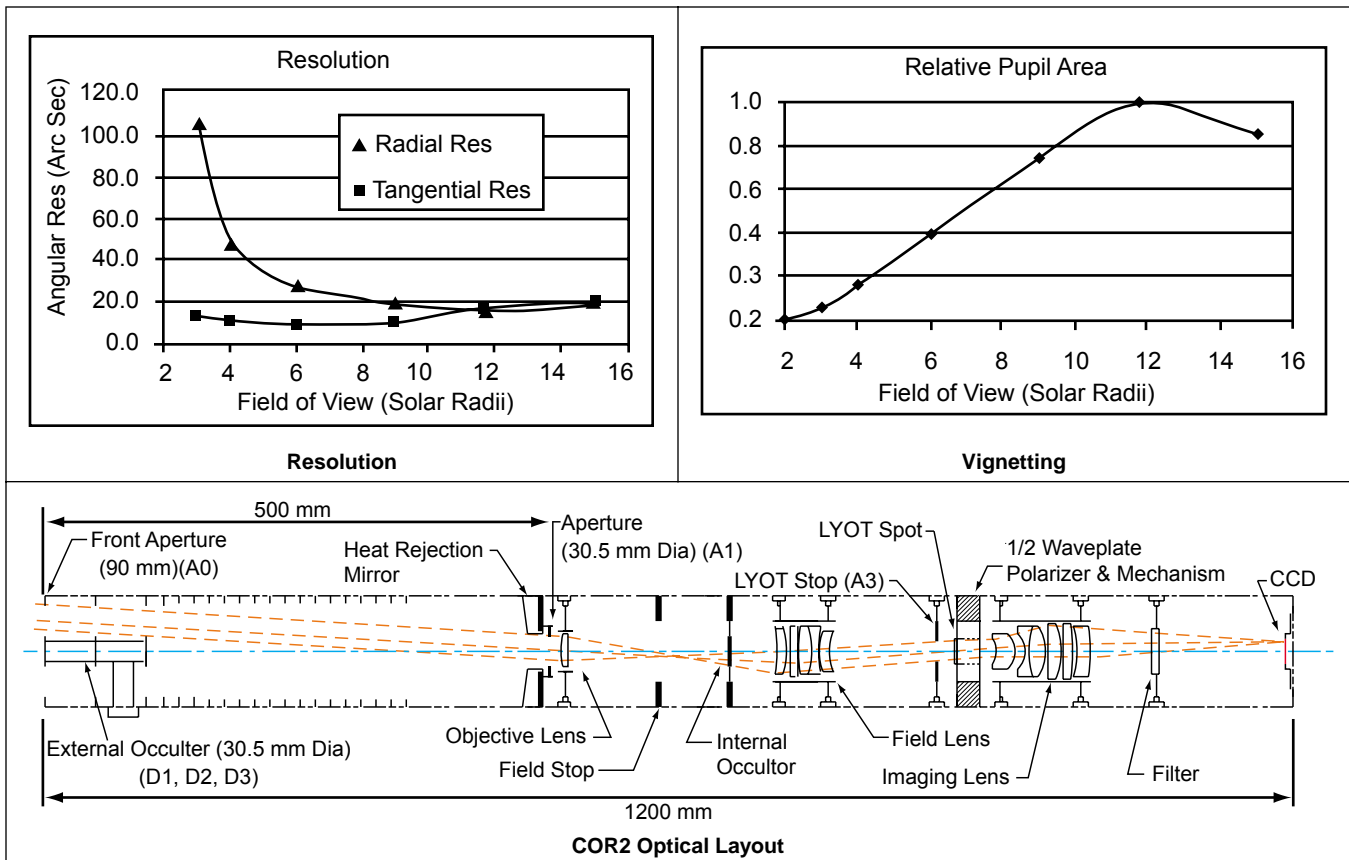


Figure 1-20. Coronagraph 2 (COR2) Instrument Parameters

the regime of COR2 will enable much shorter exposure times that were possible in C3. We estimate that the exposures will be about 3 seconds. The optical prescription was developed by Tropel who made the LASCO/C3 optics. Figure 1-20 shows the resolution of the optical system as determined by a ray trace. The difference between the radial and tangential resolution is a result of the vignetting caused by the external occulter which creates a lune shaped aperture. Figure 1-20 gives the vignetting function. The roll-off after 12 R_{\odot} is due to a small A0 aperture to keep the overall cross-section of the instrument as small as possible to fit on the STEREO S/C. This roll-off is acceptable.

□ **Passband:** LASCO used a variety of color filters to help in the separation of K- and F-coronae. An improved F-corona model has been developed so that variable passbands are not necessary for SECCHI. COR2 will have the fixed passband, 450-750 nm. This is the same passband as the HI to simplify the comparison in the region of overlapping fields. This includes the COR1 band, to ensure the continuity of observations between the two telescopes, but extends into the blue. Differ-

ences between the two instruments can be used to analyze the color of sun-grazing comets.

□ **Calibration:** The COR2 stray light levels will be evaluated in the stray light test chamber developed for the SOHO program. A source 10 m away simulates the spectrum and angular size of the Sun. In addition, we have developed many procedures for LASCO flat field calibration and for in-flight calibration against the stars. Together these procedures determine the stray light, geometric distortion, vignetting, absolute photometry and the instrument pointing and roll.

□ **Observing Strategy:** A full COR2 pB sequence will take 25 seconds (3 x exposure time + 2 x read-out time). This will permit about 9 exposures of a CME moving at 800 km/s across the field. This combined with the EUVI and COR1 observations will generate good velocity profiles for CMEs. Motions faster than 410 km/s will have moved 1pixel in the time of the pB sequence. Thus for most CMEs, it will be necessary to sum pixels (on the ground) to perform full polarization analysis. The COR2 can be used to determine the presence of a halo or other type of CME by summing up the

three pB images into a single total B image and performing an image motion analysis (already developed). It is necessary to convert to total B because pB favors observations on the limb (90E to the observer).

c. Inner Coronagraph. The Inner Coronagraph (COR1) is a low risk, classical, all-refractive design which is broadband, fast, with generous alignment tolerances, using common optical components and materials.

□ *Description and Concept:* The COR1 design combines an internally occulted coronagraph and a linear Stokes polarimeter. It is based on the successful Mauna Loa Mark III k-coronameter and the SPARTAN 201 White Light Coronagraph (WLC) polarization analysis system. The coronagraph objective lens forms an intermediate image ($f/10$) of the Sun at the internal occulter which removes the solar light inside $1.1 R_{\odot}$ while passing the coronal image from 1.1 to $4 R_{\odot}$ through the field lens onto a Lyot stop. The Lyot stop removes diffracted light and ghost images. The relay optics (doublet 1 and 2) form a simple telephoto lens, correcting the axial color and spherical aberration of the objective, and magnifying the image. The corona, geometrically centered on the solar disk, is then imaged ($f/20$) onto the CCD detector. The 2048×2048 pixels of the CCD will be binned on-chip to simulate a 1024×1024 detector area to reduce readout time to 4 seconds. This binning will also increase the effective full well. The COR1 optics provide sufficient resolution to allow imaging at the single pixel level (3.75 arcsec) for special observation programs. Integration times will vary from less than 1 second to about 4 seconds depending upon the SNR desired.

The optical design (see Figure 1-21) features a 36 mm singlet objective made of a radiation resistant, super polished, bubble-free Schott BK7. The objective forms an elongated, chromatic image of the sun onto a 35 mm long ribbed occulter supported through the center of the field lens. The occulter ribs block out-of-bandpass rays in the regime that could still leak through the filter and be detected by the CCD. The occulter has a silvered mirror on the tip that is set at a 45 degree angle; 90% of the Sun light from the solar image reflects off of the tip of occulter into a light trap and 10% is absorbed producing heat. The reflected light passes through the hole in the baffle (Figure 1-21) and through the hole in the enclosure. Then, in the

light trap, 90% of the incoming beam reflects off of the silvered, super polished fold mirror; about 10% reflects off of the highly specular black mirror (e.g., black nickel) finally to be absorbed during multiple reflections by blackened, specular (painted, e.g., black silicate paint) angled vanes in the arched cover. Enough high-loss reflections will occur to suppress the solar light to well below the level of the coronal light at $2 R_{\odot}$.

Removing the heat from the occulter assembly while keeping the field lens temperature gradients within acceptable limits presents a design challenge. The heat will be conducted to a radiator on the tube structure. Making the occulter out of glass is also an option for further study and analysis in Phase A. The rest of the occulter will be made of titanium tube with a thermal isolation mount passing through the field lens. The occulter will be radiatively coupled to a baffle mounted forward of the field lens to minimize temperature gradients in the lens. Based on experience and preliminary calculations we expect the thermal equilibrium of the occulter tip to be below 150°C and the field lens between 30 and 35°C .

□ *Observing Strategy:* COR1 is simple to operate, yet accommodates a wide variety of observing programs. During operation, only the cadence and integration time are adjustable. The nominal cadence is one pB sequence (3 images) every 6 minutes, which is the nominal cadence of the Mauna Loa Mk III coronameter. COR2 can send all 3 images so that %p, pB, B are determined on the ground. It is estimated that 24 sec will be required to obtain a full pB sequence. As a result, blur in the pB image will be insignificant for transient apparent velocities less than 494 km/sec in the FOV of the COR1 instrument. Using a 6 minute cadence, a CME with 800 km/sec velocity in the plane of the sky will be imaged seven times as it passes through the COR1 FOV. For material moving at these speeds in the lower corona, it will be necessary to do further spatial averaging, condensing the image into 512×512 samples with a 16 arc second pixel.

1.4.4 Vector Magnetograph and Guide-scope (VMAG). The VMAG contains a fine sun sensor and a basic Stokes polarimeter/vector magnetograph in one lightweight package. It provides the fine pointing error signals that meet the requirements of the EUVI, coronagraphs, and S/C. The VMAG also provides longitudinal and trans-

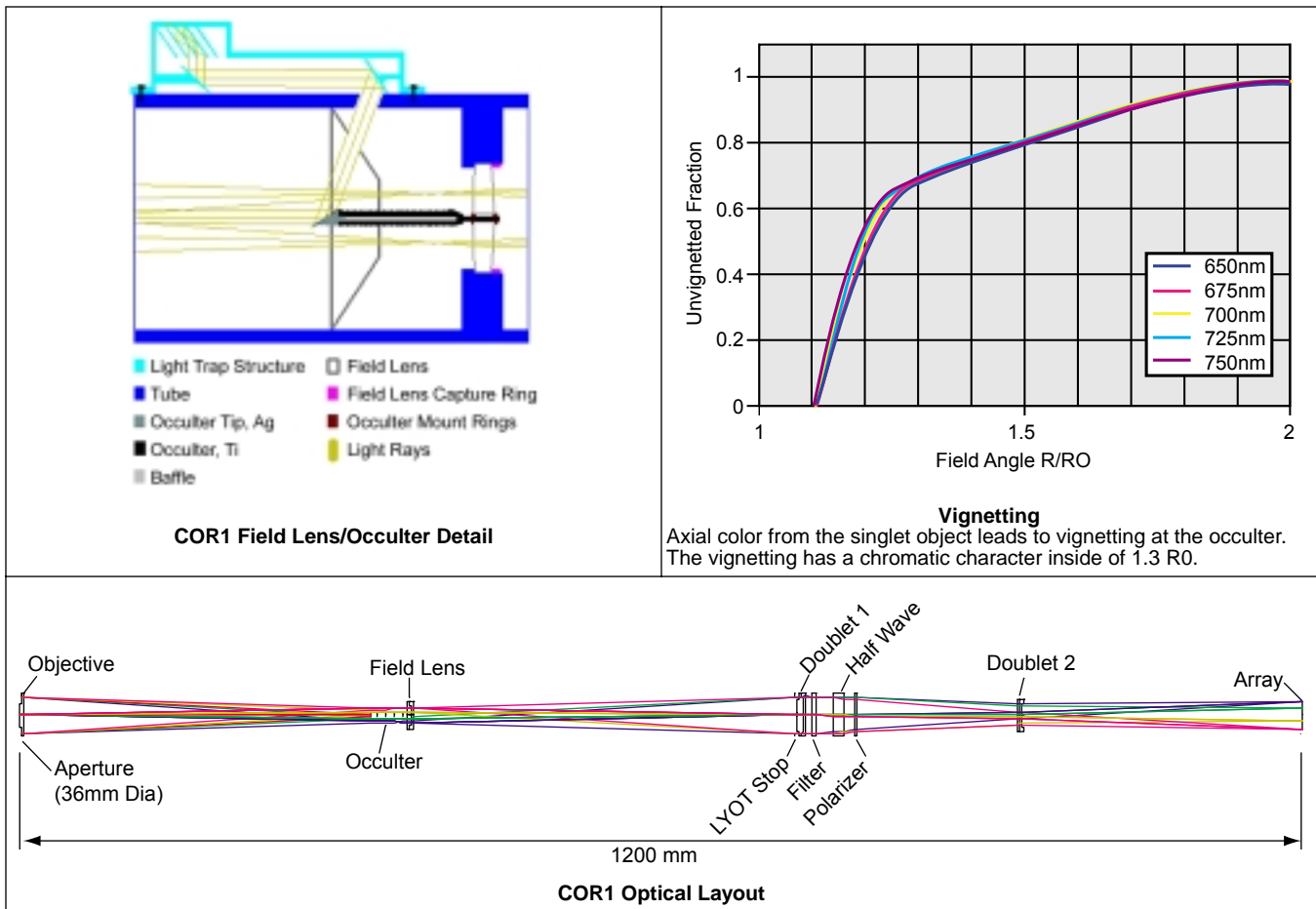


Figure 1-21. Coronagraph 1 (COR1) Instrument Parameters

verse magnetograms comparable in quality to MDI full disk images. The highly reliable instrument incorporates flight-proven MDI and TRACE designs and components (Scherrer et al. 1995; Handy et al. 1999). The sun sensor is a copy of the MDI and TRACE sun sensors, with over four years of combined on orbit operation. In a manner identical to TRACE, it provides a fast analog jitter signal to the EUV telescope and a slower digital signal to the S/C. The polarimeter implements the simple but effective HAO ASP and Solar-B designs using a proven MDI mechanism; with this approach, the vector capability requires no additional flight hardware beyond that of a longitudinal magnetograph. The narrow band filter is a solid Fabry-Perot double etalon rather than MDI's Michelson interferometers to save mass, power and cost. It operates at a fixed wavelength in the wing of Fe I 630.25 nm, which is magnetically more sensitive than the Ni I line used by MDI. The Stokes parameters IQUV are measured with an accuracy of about 0.002 of I_0 , and are processed into

vector magnetograms using the same techniques as the pioneering MSFC instrument. The calibration function relating the magnetic field to the polarization at the observation wavelength is well understood (e.g., Jefferies, Lites, and Skumanich, 1989; Klimchuk, Canfield, and Rhoads, 1992). It will be verified by simultaneous vector field observations with the Spectro-Polarimeter on Solar-B, essentially an HAO ASP in space, which observes in the same line with full spectral coverage and higher resolution and precision.

□ *Telescope and Filters:* Figure 1-22 shows a VMAG schematic diagram. The two-lens telescope has a slightly aspheric objective lens that gives diffraction-limited imaging over the entire solar disk at 630 nm. The focal length is chosen to sample this image quality while using 2x2 summing on the CCD to double the polarimetric accuracy; the result is a focal length of 268 cm, which gives summed pixels 2.08 arcseconds on a side. The element separation in this f/67 optical system is uncritical (70.2 mm) and easily met by the SEC-

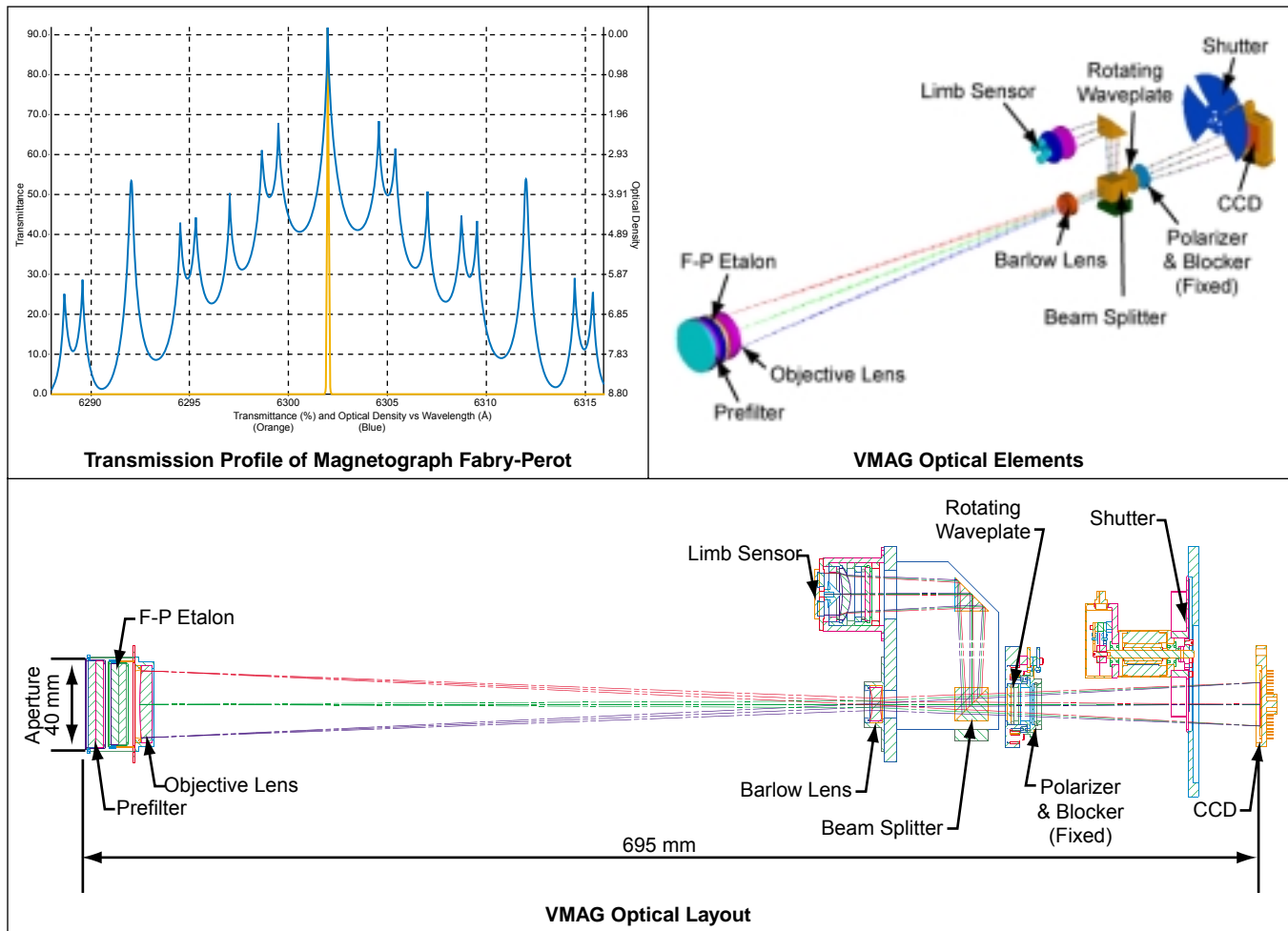


Figure 1-22. Vector Magnetograph and Guide (VMAG) Scope Instrument Parameters

CHI structure. The front window follows the MDI design, with a dielectric interference filter sandwiched between red and yellow glass plates. The resulting transmission profile admits light only between about 550 and 650 nm, 0.1 W of the total 1.7 W incident on the window. In 3 years, the transmission of the MDI window has changed less than 10%. The Fabry-Perot interferometer is a solid, double etalon, made with dielectric stack mirrors on substrates of fused silica; the transmission profile shown in Figure 1-22 (both log and linear curves) has a FWHM of about 100 mÅ at 630 nm. The mirror coatings are designed to have high reflectivity only in 600 - 660 nm, so that yellow light between 550 and 600 nm is transmitted for the sun sensor. Etalons of this type were built in the Skylab ATM program and in Lockheed-Martin IR programs for remote sensing of the upper atmosphere. The etalon has a temperature sensitivity of about 0.005 nm per degree C; its temperature is controlled on-orbit to about 1 degree, to place it in the

spectral line at the proper wavelength offset from line center. The front window and primary lens act as windows for the oven-like enclosure containing the etalon, and heaters wrapped around the circumference maintain the temperature via a closed-loop controller. Occasionally, the temperature set-point will be varied continuously over a range of a few degrees, to scan the etalon in wavelength through the line profile to calibrate the filter.

☐ *Sun Sensor*: The converging beam is split ~50-50 between the two focal planes by a low polarization beam splitter. A telecentric corrector lens in the sun sensor path reimages the pupil to infinity, making the error signal extremely insensitive to errors of focus and alignment in the telescope. The sun sensor uses the image of the solar limb projected onto four diodes in orthogonal quadrants; the intensity difference between opposite diodes is the error signal. (Redundant diodes are included, though none has ever failed on MDI or TRACE.) Modelling and in-flight calibration on MDI and

TRACE show that the signal has a linear range of ± 120 arcseconds and sensitivity of ~ 0.01 arcseconds. For SECCHI, the range will be increased by a slight change in diode geometry to accommodate the greater variation in solar angular diameter during the mission. Each diode gain is carefully calibrated in ground testing; the TRACE gains have not changed significantly since delivery of the instrument. For the EUVI image stabilization system, analog error signals are conditioned and sent to the servo exactly as on TRACE. For the S/C error signal, the analog signal is digitized at 50 Hz and averaged down to 10 Hz to reduce aliasing.

□ *Magnetograph:* The VMAG measures polarization using the ASP technique (Lites, 1994). The optical elements are simple and robust, the modulation efficiency is close to the theoretical maximum, and all four Stokes parameters are sampled by the same pixels of the same detector. The polarization modulator is a 1.35 wave retarder at 630 nm, which can be rotated to any angular setting θ with precise repeatability. The rotating retarder and the following fixed polarizer convert the states of linear polarization (Q & U) and circular polarization (V) into sinusoidal variations of intensity with θ . Stokes V, Q, and U are encoded as harmonic variations of intensity proportional to $\sin(2\theta)$, $\sin(4\theta)$, and $\sin(4\theta + 22.5 \text{ degrees})$, respectively. The Stokes parameters are measured by taking 8 CCD images with the waveplate set at intervals of 22.5 degrees in θ . Each image is either added or subtracted (depending on θ) into each of four buffer memories, which accumulate I, Q, U, and V. Any instrumental polarization and cross-talk is removed in data analysis on the ground using the instrument Mueller matrix measured pre-flight. The waveplate rotator mechanism is a scaled version of the MDI Michelson tuning motors. Constant exposure times are critical in a shuttered polarimeter; the MDI shutter has a repeatability measured on orbit of much better than 50 microseconds, so the SECCHI shutter will not limit the polarimetric accuracy. Once the CCD is read out with 2x2 summing in 4 seconds, and an 8 exposure set can be done in about 33 seconds. The magnetograph path also has a blocking filter to eliminate all light except a 1 nm band centered on the solar line; it has a heater and insulation for temperature control to about $\pm 5^\circ\text{C}$. A light-level calculation shows that a single 50 ms exposure will collect about 2.2×10^5 electrons in a 2x2 summed pixel. Eight of these

yield noise in Q, U, and V of about 0.13% of the continuum intensity. Extra noise sources at the level of 0.1 - 0.2% arise because the images are separated in time and have slight spatial misalignments. The latter are removed in the onboard computer, by fractional-pixel translation (as is done in MDI); the sun sensor error signal at the time of exposure determines the shift. All of these noise sources are present and similar in MDI full disk magnetograms. They have an rms noise level of about 15 Gauss flux density or 3.0×10^{17} Mx flux. The same noise sources would produce a noise in the transverse field of order 100 G. Since the magnetograph uses a fixed wavelength, it will have varying sensitivity across the disk because of the ± 30 mÅ Doppler shifts of solar rotation.

1.4.5 Extreme Ultraviolet Imager. The EUVI observes the chromosphere and low corona in four different EUV emission lines between 17.1 and 30.4 nm. To meet the scientific objectives, the EUVI has a full sun FOV extending to 1.5 solar radii, good spatial resolution defined by 1.4 arcsec pixels, the capability to image the corona at different temperatures, and the capability for fast image cadence. The EUVI is a small Cassegrain telescope with heritage from EIT and TRACE. The EUVI's substantially improved mirror coatings and detector provide higher sensitivity, resolution, and image cadence than previously possible.

□ *Overview:* The instrument is shown in Figure 1-23, which also lists its parameters. EUV radiation enters the telescope through a segmented thin-film Al filter, 150 nm thick, supported on a mesh. This filter suppresses most of the UV, visible, and IR radiation and keeps the solar heat out of the telescope. During launch, the filter is protected by an outside door. Next the radiation passes through a sector shutter to one of the four quadrants of the optics. Each quadrant of the primary and secondary mirror is coated with a narrow band, multilayer reflective coating, optimized for one of four EUV lines. The radiation continues through a filter wheel, with redundant thin-film Aluminum filters to remove the remainder of the visible and IR radiation. A rotating blade shutter controls the exposure time. The image is formed on a CCD detector.

□ *Optics:* The thin-film filters are procured from Luxel corporation, as was the case for SXT, TRACE, and SXI. The mirrors are made of Zerodur and are super-polished to a spherical shape by General Optics company. They are then ion beam

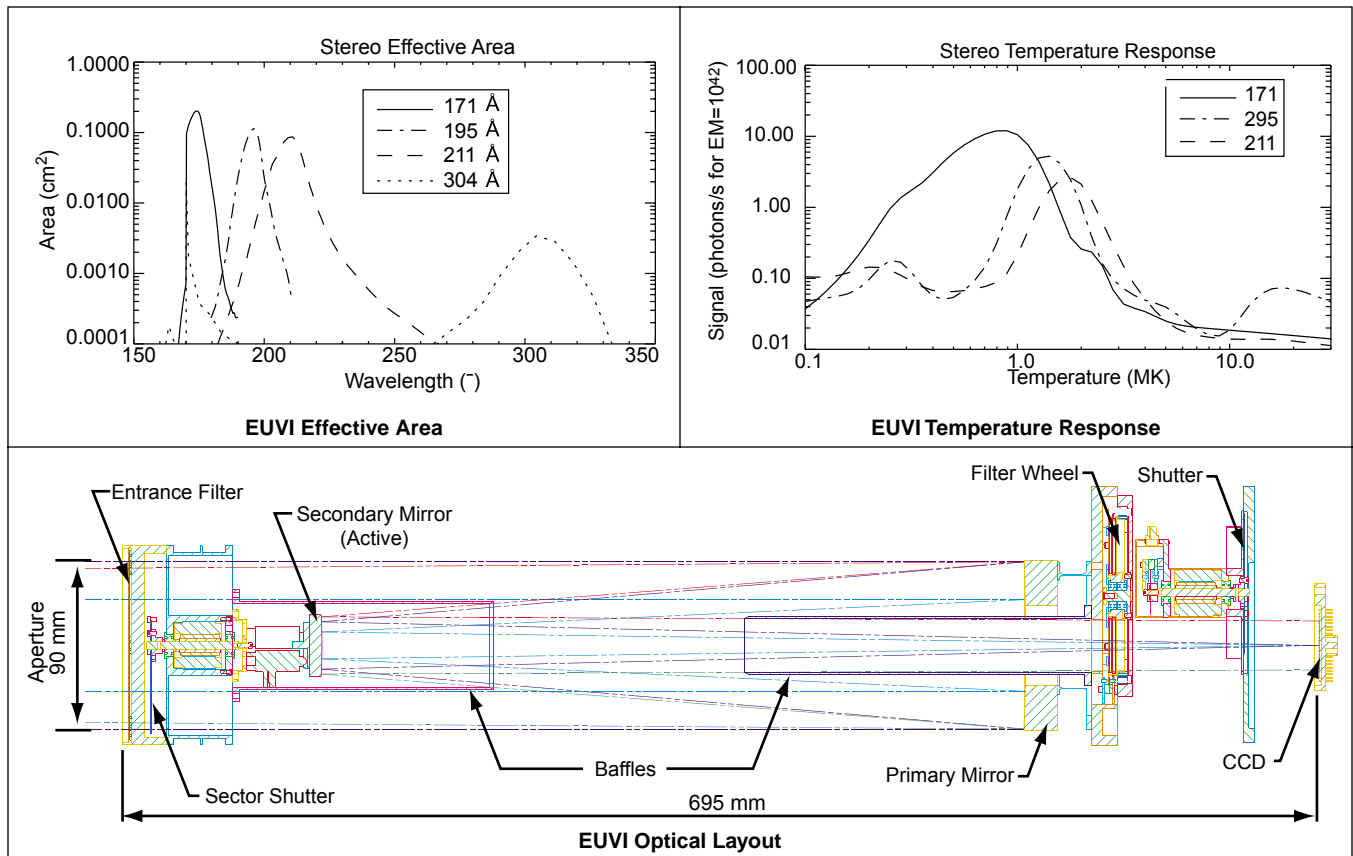


Figure 1-23. Extreme Ultraviolet Imager (EUVI) Instrument Parameters

etched to their final figure, and multilayer coated at the Centre Universitaire d'Orsay in France. The same organization produced the EIT optics. A ray trace of the EUVI optical system, set at optimum focus, shows that the spot size is less than the pixel size over the full FOV. The optics is fully baffled. The detector is a backside illuminated, backside pacified 2k x 2k CCD detector with an EUV quantum efficiency in excess of 70 percent. The baseline detector is a device from EEV, type 42-40. Near-identical devices (EEV type 42-10) have been tested extensively for both quantum efficiency (Figure 1-26), stability, and resistance to XUV radiation damage on the SXI program. On all accounts they are much superior to the detectors used on EIT or TRACE. The detector is passively cooled by a radiator.

□ *Wavelengths:* The primary candidate wavelengths for the EUVI were selected for the SECCHI science goals and are shown in Table 1-7. The corresponding instrument response curves and the detected photon flux for isothermal solar plasmas are shown in Figure 1-23. The He II 30.4 nm line images the chromosphere, and shows erupting

prominences associated with CMEs. The Fe IX 17.1 nm line shows the sharpest contrast in coronal loops, as seen in TRACE. Fe XII at 19.5 nm images the Sun at a temperature “typical” for the quiet corona, while Fe XIV at 21.1 nm images a hotter corona. Images at 21.1 nm were observed by the Japanese XDT rocket. They look similar to EIT images at 28.4 nm. The final selection of the channels will be made in phase A.

□ *Structure:* The front end of the telescope consists of the aperture door, the filter section, and the spider assembly. The filter section is not evacuated. The EUVI entrance filters are small, only about the size of similar thin-film analysis filters on SXT and TRACE, which have been launched successfully without the protection of a vacuum chamber. The filter section will be tested early in the program, to allow for design adjustments without impact on the overall program schedule.

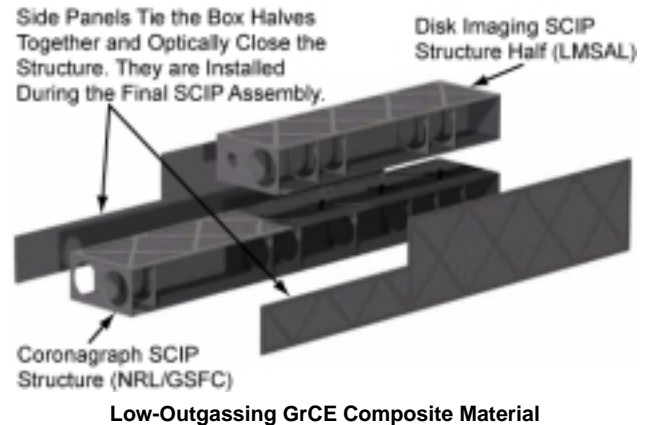
□ *Image Motion Compensation:* Since the STEREO spacecraft group cannot assure during pre-Phase A that the jitter specification can be met, the EUVI secondary mirror is actuated to compensate for S/C jitter. This image stabilization System

(ISS) is essentially identical to the one used in TRACE. It uses low voltage piezoelectric transducers, and signals from the VMAG instrument. The ISS becomes unnecessary, and can be de-scoped, with considerable savings of mass, cost, power, and risk if the S/C performance meets our jitter requirement of 1.5 arcsec (3 sigma).

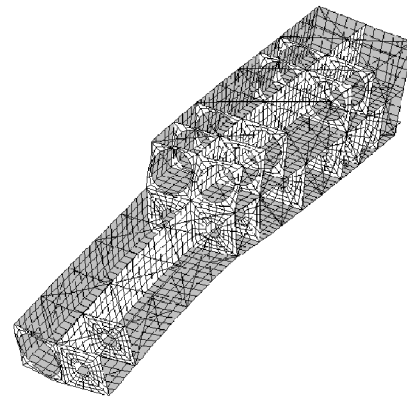
□ *Calibration Plan:* Each component of the optics is calibrated individually at EUV wavelengths. The filters are calibrated at LMSAL. The CCDs are calibrated at MSSL in Britain. The mirrors are calibrated at a synchrotron facility in France. Overall instrument alignment, focus position, out-of-band rejection, and ISS performance are calibrated at visible wavelengths at LMSAL.

1.4.6 SCIP Structure. The requirements on the optical support structures for the Sun-centered instruments listed in Table 1-7 are stringent, but within the available mass budget. The requirements include the alignment tolerances for the optical elements, telescope co-alignment, optical test and verification during S/C I&T, thermal stability of optical alignment, and retention of focus on orbit. To meet these requirements, the Sun-centered instruments were grouped together into a single structure, called the SCIP similar to the three coronagraphs that were successfully grouped in LASCO. The SCIP builds on LASCO, EIT, MDI, and TRACE designs by incorporating composite technologies to reduce mass. It uses proven spaceflight heritage materials and processes, supported by design methods and materials developed by HYTEC Corp. (a small business located in Los Alamos NM) that were demonstrated on the FORTÉ satellite launched in August 1997 (Thompson et al. 1995). HYTEC pursued a detailed analysis of several design concepts. The selected concept is simple, and employs a composite truss structure surrounding the box containing the optics. Mortise and tenon technology (proven on FORTÉ) is used to achieve joints between structural elements. It is easily fabricated, and provides stability and stiffness at relatively low cost.

□ *Background and Material Selection Process:* An in-depth evaluation was undertaken for the proposal to clarify the underlying geometry issues of the instrument suite. The analysis was based on the composite material M55J/954-3, a Graphite/Cyanate Ester (Gr/CE) resin system. Progress with these composite materials has reached a point that their outgassing properties are comparable with



Detailed Optical Box Design Reduces Development Risk



High Fidelity FEM Model Shows Primary Mode (149 Hz)

Figure 1-24. SCIP Composite Optical Box

spaceflight quality anodized aluminum. Gr/CE materials were successfully flown in the SOHO UVCS coronagraph/UV spectrograph, which has extreme sensitivity to outgassing. The UVCS success and minimal degradation demonstrates that Gr/CE structures are a low risk for both EUV imagers and coronagraphs. To further ensure minimal

contamination risk, the truss structure is located outside of the optical cavities. The truss has the majority of the high strength adhesive joints in the structure. In the conceptual design, no optical element has a line-of-sight view to one of these joints. The boxes will be vented similar to the LASCO optical box. A cleanliness and materials selection program will be initiated early in the program to assure compatibility of the selected SCIP structure materials. There are many surface options that can be employed should the materials program show the need.

□ *Thermal Expansion:* M55J has an elastic longitudinal modulus of 75 MSI. The resulting CTE will be very near zero for a quasi-isotropic (QI) lay-up. Thus, for the proposed structural design with this material, thermal stress is not an issue. The structure will not change optical alignment over the standard operating temperature range of 0C to 40C. All thermal expansion is through the thickness of the layups since in-plane growths are designed to have an effective CTE of zero. The elastic modulus through the thickness is much lower so that even if there are relatively high rates of growth they are easily constrained by the surrounding high modulus of the in-plane laminate material.

□ *Finite Element Analysis and Models:* Our design study included finite element solutions to support and optimize the SCIP optical box. A FEA was performed to estimate both the stiffness and stresses of the optical box. A modal analysis was performed on the finite element model (FEM) to assess the structural stiffness of the instrument. Component masses were included and the results show a fundamental mode of 149 Hz (see Figure 1-24). The modes are well within reasonable flight design requirements. The difference between the free-free mode study and the mode study constrained by S/C mounting supports indicates the influence of the location of the boundary support points. If they were supported as a cantilever, e.g., the frequency would be still lower. If the location of the support simulate the free-free condition it would provide the high frequency indicated, without redundant supports that may lead to undesirable strains. During Phase A, the structure will be studied in greater detail to optimize the instrument's mounting configuration.

□ *Stress Analysis:* A preliminary stress analysis was performed (see Figure 1-24) to determine the

worst case stresses experienced during launch. Worst-case launch loads were estimated using the AO's information. The maximum stress in the structure was ~20% of the material's ultimate strength, with a margin of safety of ~7.2. Detailed FEA solutions will be run during Phase A to assess the design's sensitivity to thermal variations. To achieve the required level of stability, it will be necessary to validate micron level predictions with experimental measurements during Phase B. HYTEC has developed unique hardware and software in cooperation with Los Alamos National Laboratory that is capable of measuring displacements resulting from applied loads in realtime. This capability will be used on the SCIP structure.

□ *Mass Estimate:* Mass calculations for the design, including structural contingency in the calculations, show 3.95 kg for M55J/954-3. Further analyses during Phase A will focus on minimizing mass while maintaining the structural integrity and optical stability of the package.

1.4.7 SECCHI Electronics Box. The instrument suite (SCIP and HI) consists of five telescopes, five CCDs, two cameras, and a SECCHI Electronics Box (SEB). Figure 1-25.(a) provides a block diagram of the instrument suite and its electronics. The SEB is the only electronic interface with the S/C. Our design partitioning optimizes command and data handling (C&DH) capabilities within the specified S/C resources. Additionally, the processing electronics are housed within a single heritage box that is the responsibility of LM-SAL. Nearly every SEB circuit is a copy or modest modification of circuitry used in the SXI, TRACE, and MDI, or circuitry under development for LM-SAL's Solar-B focal plane package. The camera readout electronics and their power circuits are housed close to the CCDs to minimize mass and power inefficiencies (see Section 1.4.8).

□ *SEB Overview:* The SEB consists of a control computer, interfaces for the camera and CCD, fine pointing and jitter control electronics, mechanism drive circuits, a housekeeping data acquisition system, S/C interfaces, and power conversion. It is built using a Lockheed-Martin Federal Systems RAD6000 33 MHz RISC-based single board computer (SBC) that was developed specifically for the SXI program and will be used *without change* in SECCHI. The SBC uses a PCI bus and four High Speed Serial Interfaces (HSSI) to control the SEB's circuit card assemblies (CCA). The SBC is

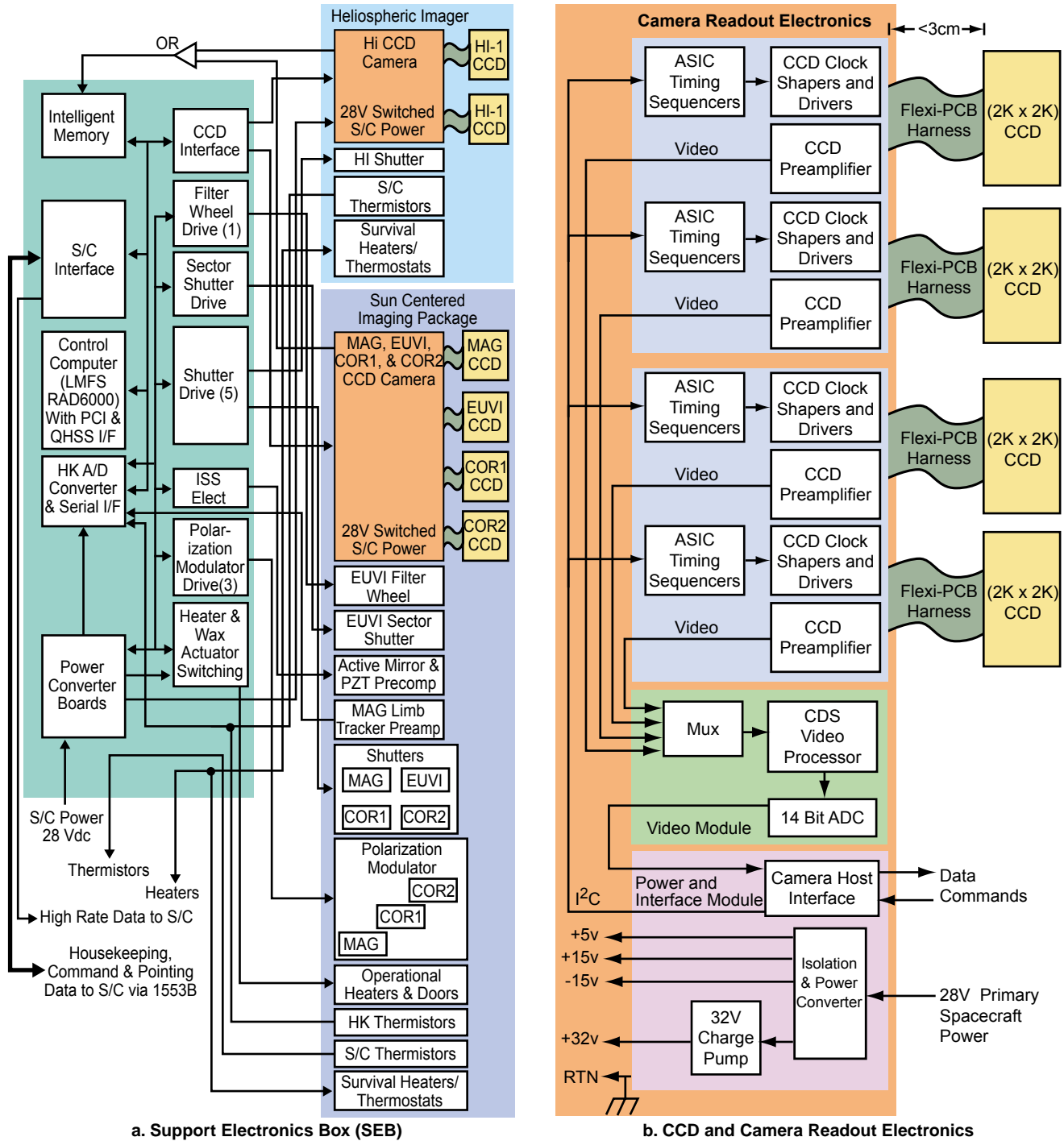


Figure 1-25. SECCHI Electronics Box (SEB) and Camera Readout Electronics Block Diagram

fast enough to provide data compression even during rapid flare observations.

□ *Spacecraft Interface CCA:* The SEB has two interfaces to the S/C, and the S/C interfaces are contained on a single CCA that connects to the SBC via the PCI bus. A 1553B Bus Remote Terminal interface receives S/C commands and provides

low-rate housekeeping telemetry data to the S/C. TRACE uses a similar 1553B configuration, and the handshaking conventions are well understood. An RS-422 interface provides the high-rate data telemetry interface over which compressed CCD camera image data is passed to the S/C.

□ *Housekeeping CCA*: The SEB collects, digitizes, and sends selected voltages, currents, and thermal sensor monitors to the S/C via the Housekeeping CCA. It also contains a serial interface that supports the mechanism driver modules and sends commands to the CCD camera electronics. The housekeeping ADC is contained on another CCA that also connects to the SBC via the PCI bus.

□ *Mechanism Drive Electronics*: The drive electronics for the 10 SECCHI mechanisms reside on 3 CCAs, and use the equivalent space of 2.5 CCAs. EUVI uses one filter wheel drive and one sector shutter drive; shutter drives are provided for the SCIP (4) and for the HI (1); and polarization modulator drives are provided, one each for the COR1 and COR2, and one for the VMAG. These mechanism drives will be nearly identical copies to ones used on MDI, TRACE, and SXI.

□ *Image Stabilization System*: The ISS is very similar to that of the TRACE telescope. Analog error signals are amplified, conditioned, and used to drive a set of three low-voltage piezoelectric transducers (PZT) that orient the active mirror. The ISS electronics includes two preamps in the imaging package: one for the magnetograph's limb tracker photodiodes, and one for the position sensors of the EUVI active secondary mirror. The ISS electronics are well-understood with versions operating in TRACE and MDI.

□ *Intelligent Memory Buffer CCA*: The CCD camera output data from the camera readout electronics goes to the memory buffer CCA that can perform single add, subtract, and load complement instructions. This permits simple preprocessing before the RAD6000 compresses the data. We performed data flow studies, and confirmed that standard and high rate scientific sequences can be performed at the AO's mass memory transfer rate using only 50% of the available processor cycles.

□ *Power Control, Conversion, and Heater CCA*: The power system uses standard modular power converters and EMI filters. It will be similar to those on SXI and TRACE, and makes use of off-the-shelf Interpoint converters and the appropriate filtering circuitry. The output voltages are distributed by the power and heater control CCA that also contains the paraffin actuator drive circuits for one-time door mechanisms. These techniques were used in the TRACE and SXI electronics.

1.4.8 SECCHI Camera System. The SECCHI camera system uses existing CCD detector designs

from EEV Ltd. for the SCIP and the HI. The camera readout electronics are directly based on a design for SMEI, and the camera readout electronics for each SECCHI instrument will be of common specification. This heritage and commonality minimize schedule and design risk for the mission.

□ *CCD Detectors*: The CCDs are thinned, back-illuminated, low dark current variants of the EEV CCD42-40 (2k x 2k pixels). The VMAG, COR1/COR2 and HI will employ standard anti-reflection coated CCDs. The EUVI telescope will be fitted with a bare (non-coated) CCD with excellent response at EUV wavelengths. Each camera head unit consists of a CCD chip mounted on a cold-finger linkage to an external radiator.

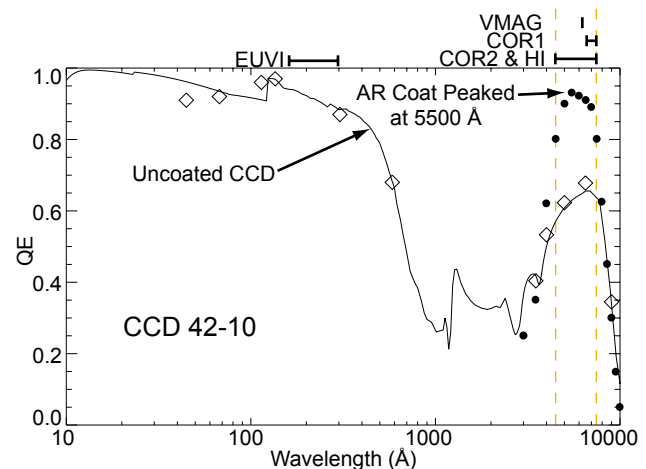


Figure 1-26. Measurements of the Quantum Efficiency of a UV Enhanced CCD. No Anti-Reflection Coating is Used on the EUVI Detector.

□ *Camera Readout Electronics*: Each instrument's camera readout electronics are required to read out its CCD at 0.5 Mpixels per second and to digitize the resultant video signal to 14 bits accuracy. The electronics timing will be designed around an ASIC CCD waveform generator and sequencer previously developed by RAL and used in SMEI. The ASIC provides all the programmable timing control required to read out the CCD, and a serial command and data link with the SEB. The readout electronics for the SCIP is mounted in a single box on the aft wall of the structure. The distance between any CCD and the electronics module is less than 3 cm and the 4 CCDs are connected to the readout electronics via a short flexi-PCB minimizing harness mass. This is the same design previously used in LASCO and EIT cameras. Figure 1-25(b) illustrates the functionality of the basic CCD

drive circuitry. The readout electronics for the two HI cameras are mounted in a single box between the cameras to obtain a short cable run to the CCD. The HI interfaces directly to the SEB for command, data, and 28 V power. There are separate power converters in each camera electronics box to minimize ground loops and noise problems. Figure 1-25(b) shows the camera system's layout.

1.4.9 Mechanisms. The SECCHI mechanisms, exclusive of the doors, will be provided by LMSAL and are scaled versions of similar mechanisms on MDI, TRACE, SXI, and EPIC. The fundamental design, performance, and life test of such mechanisms during the MDI program is described in Akin, Horber, and Wolfson (1993).

□ *Focal Plane Shutters:* Each telescope contains a focal plane shutter in front of the CCD camera; and all shutters are identical. The two HI optical paths are controlled by a single shutter mechanism. In addition, the EUVI sector shutter is a scaled version of the focal plane shutters design. Mechanisms use a brushless DC motor with an integral, optical, shaft angle encoder that provides position feedback for commutating the motor and measurement of the actual exposure. The MDI prototype underwent a life test of 67 million exposures and the flight unit has taken more than 20 million images. The TRACE shutter has taken more than 2 million exposures, and the SXI prototype completed a life test of 30 million cycles.

□ *Rotating Waveplates:* The three rotating waveplates are scaled versions of motors on MDI and TRACE. They are brushless DC motors designed and built by H. Magnetics in close coordination with LMSAL. The MDI prototype motor underwent a life test of 100 million cycles and the pair of units on MDI have made over 20 million moves. As with the shutter motor, an integral, optical, shaft angle encoder is used for commutation and for identifying the position.

□ *Filterwheel:* The EUVI uses a scaled version of heritage filterwheels with improvements from SXI. SECCHI's on orbit usage is less than MDI and TRACE where no on orbit problems were encountered. MDI underwent a 67 million cycle life test, and SXI underwent a 30 million cycle test.

□ *Lubricants:* The shutter mechanisms use a Bray 815Z oil, while Braycote 600 grease is used in the rotating waveplates and filterwheels. These lubricants underwent outgassing testing at LMSAL, and the Lyman Alpha channel on TRACE

has shown no significant degradation from outgassing in 15 months.

□ *Doors:* The SCIP doors will be provided by MPAe (design) and the University of Keil (fabrication and test). The baseline design will be a duplicate of the LASCO doors (MPAe) with the motors removed. The doors open when the paraffin wax-actuated fail-safe device is enabled. Refinements to the baseline design will be made to reduce the devices weight and complexity.

1.4.10 Thermal Control System. The SCIP, HI and SEB units use a passive TCS to maintain unit temperatures within limits. The design incorporates the same principles implemented on LASCO, EIT, and MDI. The individual units will be thermally isolated from the S/C. The CCDs will be passively cooled to -60°C with a $\sim 250\text{ cm}^2$ radiator per chipset (similar to LASCO's camera design). Both the HI and SCIP CCD radiators are installed at the rear of the instrument and will have a clear view to space. The SCIP TCS will maintain the optical box to $\sim 10^{\circ}\text{C}$ during normal operations. Dissipated heat and absorbed solar energy will be matched by radiative losses through the front aperture and blankets. The dissipated energy will be spread through the box with radiative and conductive coupling. About 3W heater power is required to offset SCIP uncertainties in MLI, BOL/EOL properties, and variations in the solar constant. The HI will use the dissipated power in the CCD cameras to warm the optical telescopes, and the baffle structure will be biased cold. The SEB will be cooled using a radiator that views deep space. A thermal balance test will be conducted to validate the thermal design.

1.4.11 SECCHI Flight Software. Our FSW approach builds on many years of experience gained from previous instrument programs like LASCO, EIT, MDI, and TRACE. Substantial code is available to this consortium from the GSFC and LMSAL *Triana*, LMSAL's SXI for NOAA GOES, and the GSFC SMEX light and SPARTAN programs. These existing resources allow maximum reuse to minimize cost, schedule and risk. We will use a proven COTS O/S (*VxWorks*) to provide a multitasking, preemptive real-time O/S. Its modular design allows testbed configurations that communicate to external test and development systems using common protocols for easy debugging. New FSW will be written in C and C++.

❑ *Memory Margins:* FSW executes from the RAD6000 (see Section 1.4.7) from 8 MB of system RAM that may be loaded from one of two EEPROM areas. The first area is 1 MB in size and contains minimum core C&DH functionality and safehold processing. This area cannot be modified in-flight. The second area contains the full-up FSW load, and may be modified in-flight to handle contingencies. Roughly 88% (999kB or 1,060kB with 15% reserve) of the instrument’s FSW exists; the remaining 12% (125kB based on LASCO FSW) will be developed specifically for SECCHI. This provides a 44% margin for fitting within the RAD6000 processor memory.

❑ *Processor Margins:* The processor usage is shown in Table 1-8. The amount of image processing is configurable in-flight and can accommodate new processing modes as compression algorithms mature.

Table 1-8. SECCHI Processor Usage

Experiment Mode	MIPS	MIPS + 15% Reserve
C&DH	3.0	3.5
Experiment	3.5	4.0
Image Processing	3.5	4.0
Margin	—	18.5
Total	10.0	30.0

❑ *Health and Safety:* Voltage, S/C pointing, and temperature limits are monitored to ensure safe conditions. The FSW can safe the instrument if an error is detected or if self-test fails. Should the guide telescope error exceed a designated threshold, the instrument suite is automatically safed.

❑ *FSW Design:* The architecture reuses the SPARTAN multitasking design architecture to lower cost and reduce risk. Table 1-9 lists major FSW tasks and their functions.

❑ *Image Processing and Data Compression:* Substantial reuse of existing S/W is planned for the image processing and compression FSW, using routines developed for LASCO. These routines are reusable with minor modifications, and include summing and differencing of images, pixel summing, cosmic ray removal, and region of interest masks. Existing compression routines include both a lossless (Rice) and a lossy wavelet compression (H-compress). Compression factors of 1.75 to 2.5 for the lossless approach and higher compression ratios (5-10x) using H-compress are achievable. At the 6x compression, H-compress achieves approx-

imately 0.1% photometric accuracy. Compression by masking and binning (used on LASCO) in combination with lossless compression is predicted to give compression factors of up to 7. Transmitting the image in independent pixel blocks (32 x 32) insures image integrity if telemetry packets are lost. With the RAD-6000 processor, 5 seconds are required to compress 1 MB based on a comparative analysis between the LASCO processor and the RAD-6000 processor. The time to compress a baseline observing plan that generates 4.4 GB of raw data or 450 MB of compressed science telemetry per 24 hours requires ~22,000 seconds during the course of the day.

Table 1-9. Flight Software Developmental Status

Subsystem	Function	Status and Source	KBytes of RAM	
			Reuse or Modified	New
Task Manager	<ul style="list-style-type: none"> Add or Destroy FSW tasks 	Direct Reuse from GSFC's SPARTAN	12	
Scheduler	<ul style="list-style-type: none"> Ground Commands HK commands Timed I/O ops 		16	
File Manager	<ul style="list-style-type: none"> File Transfer via QHSS to S/C 	Modified from GSFC's SPARTAN by NRL	20	
House keeping	<ul style="list-style-type: none"> Receive HK from other S/W Subsystems WDT Reset Send HK to S/C 		11	
Flight Software Manager	<ul style="list-style-type: none"> Load or Dump System Tables or Memory 	Direct Reuse from GSFC's SPARTAN	27	
Self Test	<ul style="list-style-type: none"> Power on tests 		38	
Ext. Bus Remote Terminal	<ul style="list-style-type: none"> 1553 Bus 		4	
Checksum	<ul style="list-style-type: none"> Periodic Checksum of Tables or Memory and error detection 	Direct Reuse from GSFC's SPARTAN	7	
Memory Scrub	<ul style="list-style-type: none"> Error Detect and Correct Memory 		9	
Software Bus Library	<ul style="list-style-type: none"> Route Data over FSW bus 		142	
Experiment Control	<ul style="list-style-type: none"> Instrument Support Functions 	New Development by NRL		60
Experiment Science Processing	<ul style="list-style-type: none"> Output SECCHI Science Data 			45
Experiment House keeping	<ul style="list-style-type: none"> Output SECCHI Housekeeping Data 			20
Totals			286	125

1.5 Spacecraft Accommodations. The SECCHI instrument suite fits within the S/C resources.

□ *Interfaces:* There are three primary mechanical and thermal interfaces with the S/C (HI, SCIP, and SEB), and one electrical interface (SEB). All inter-instrument electrical interconnects are provided by a SECCHI flight harness. We will reuse LASCO and EIT practices where intra-instrument interfaces were controlled via the Consortium Interface Memoranda. These define the mechanical, optical, thermal, and electrical interfaces of the instruments. They permit development work for each instrument to proceed in parallel, and ensured compatibility of the EMs, QMs, and FMs. The memoranda formed the basis of Interface Control Documents (ICDs) administered by NRL with the instrument developer's concurrence. Drafted in Phase A and finalized in Phase B, these ICDs establish the basis and coordination with the S/C accommodation.

□ *Power and Thermal Interfaces:* SECCHI's SEB meets the AO's electrical, data, and bus specifications with a single interface to the S/C. The SEB is thermally isolated from the S/C, and its location on the S/C is constrained only by the allocated harness mass.

□ *Mass and Power:* The SECCHI instrument suite's meets the AO's mass and power requirements (see Table 1-11), and detailed parameters for each component are presented in Table 1-11. Mass and power contingencies are explicitly listed. Component contingencies were assigned based on heritage.

□ *Reliability Assurance:* All EEE parts, CCDs, and optics meet a >10 K RAD (Si) radiation environment. A worst-case analysis and parts-stress derating is performed on all electronics.

□ *Cleanliness and Contamination Sources:* Both particulate and volatile contamination must be considered, and a stringent materials selection process is required, with system-level bakeouts. Contamination control practices are required for all assembly, integration, and test activities involving the instrument suite. Instrument integration will require a Class 10,000 clean room with localized purges. The location of the instrument's optics makes them relatively immune to S/C cold-gas plumes degradation.

□ *Alignment and Field of Regard:* The HI and the SCIP must be boresighted to one another within 30 arc-minutes using the optical reference cubes on

each instrument (see Section 1.7). The COR1 and COR2 minimum FOV is 150°, while the HI's designed clear FOV is a 2π hemisphere. However, the HI's unique optical design makes possible exceptions to this clear FOR beyond 90° from the earth-Sun line. Note that no exceptions can be made for a HI design viewing of a full 180° FOV vs. the proposed 85° FOV.

□ *Pointing Control:* The minimum required long-term pointing control of 2 arcsec is determined by the need to have a constant stray light pattern in the coronagraphs. As described in Section 1.4.2 and demonstrated with LASCO, only with a constant stray light pattern can a model be constructed to remove the straylight component remaining after all other techniques have been applied. Given the pointing signal from the VMAG, the STEREO AO Q&A page indicates that this pointing can be achieved.

□ *Jitter:* Our uncertainty about the S/C's capability to accommodate the jitter budget was mitigated by including Image Motion Compensation (IMC) in the EUVI, with impacts on the SCIP's mass and cost. If the jitter budget can be accommodated by the S/C, no IMC will be required.

□ *Launch Accommodations:* We evaluated alternate launch envelopes and came to the same conclusion as expressed in APL's report—the *Athena II* is the smallest vehicle to accommodate a STEREO launch. Our proposed instrument configuration uses that vehicle's envelope for the most volume constrained mission (see Table 1-4).

1.6 Development Approach. The breadth of expertise and facilities resident in the SECCHI consortium allows a low-risk development. Development of the instruments will be undertaken in parallel with coordination by the Program Scientist, System Engineer, and Program Manager (see Section 4.2.2).

□ *Telescope Development and Calibration:* The design, fabrication and testing for each telescope optics set will be accomplished by the responsible institution (see Table 4-2). The HI instrument development effort will proceed largely independent of the SCIP telescopes. Each SCIP telescope team will receive a duplicate of the composite structure Engineering Model (EM) that will be resident at their laboratory throughout the program (see Figure 1-27). Interface "fit-checks" and optical test procedures development is accomplished using the EM. The telescope teams will also have EM cam-

Table 1-10. SECCHI Instrument Suite Power

Component	Heritage	% Reserve	Power w/ Reserve (W)	
			Reg'ltd	UnReg'ltd
SECCHI Electronics Box (SEB)				
CPU	SXI	0	7.0	
Smart Memory	Solar-B	10	1.1	
S/C Interface	SXI Mod	10	1.4	
Housekeeping	Solar-B	10	1.4	
Mech. Controllers	SXI	0	0.3	
PWR & Thrm'l Cntrl	SXI Mod	10	0.4	
IMC	TRACE	0	1.0	
SCIP Optics Box Electronics				
Limb Sensor PreAmps	MDI TRACE	0	0.5	
PZT Strain Gage PreAmps	TRACE	0	0.5	
SCIP Optics Heaters	-			3.0
Subtotal			13.7	3.0
SCIP Camera				
Drivers, Clocks, Pre-Amps; Mux, CDS & 14 bit ADC; Cam R/O Unit; & Pwr Cnvtr CCA	SMEI Dev'l	15%	6.2	
HI Camera				
Drivers, Clocks, Pre-Amps; Mux, CDS & 14 bit ADC; Cam R/O Unit; & Pwr Cnvtr CCA	SMEI Dev'l	15%	5.0	
HI Optics Heaters	-			1.5
Total, Regulated Power			24.8	
Converter Efficiency @ 70%			35.4	
Total, Regulated and Unregulated Power			39.9	

eras available for this testing. The performance of EM and Flight Model (FM) optics will be verified using the EM, while the principal validation, characterization, and calibration of the FM optical telescopes will be undertaken in the FM structure prior to its delivery to NRL. The EM camera is replaced by the FM camera before delivery to NRL. Final end-to-end instrument calibration uses unique optical facilities (see Table 4-5) at each institution. Subsequent optical tests at NRL with the integrated instrument suite will validate calibration and measure any changes that may have occurred. Each team is responsible for developing integrated instrument test scenarios, and the tests performed during payload-to-S/C integration.

❑ *Mechanisms, SEB, Flight Software, and Cameras:* These developments proceed in parallel at each responsible institution. Each component has considerable flight heritage. Mechanisms are

based on designs from LASCO, EIT, TRACE, and MDI. The SEB is nearly identical to the SXI unit. FSW reuses existing modules, with appropriate updates specific to the SECCHI. The writing and initial testing of the FSW is done on a *PCPlus* development system that simulates the inputs and outputs of the SEB, mechanisms, and cameras. This development station will be progressively upgraded and the final version will incorporate the SEB driving high fidelity mechanism and camera simulators. The camera is based on the SMEI design. ASRG will qualify the camera as a new sub-assembly with a progression of an EM, an Environmental Qualification Model (EQM), and a FM. All subassemblies will be developed and tested according to established procedures (used on LASCO, EIT, MDI, TRACE, and SMEI) with updates to accommodate SECCHI and the STEREO needs.

❑ *Development and Qualification Testing:* Our structural qualification approach uses extensive computer modeling and validation testing based on guidelines from GSFC's *Environmental Verification Specification for ELV Payloads* (GEVS-SE). Specifications from the S/C developer and ICDs define vibration, shock, and thermal environments that are used to develop qualification test approaches. The SCIP and HI primary structure will be qualified by Structural Model (SM) testing using mass simulators for select components. Similarly, thermal modeling will define specifications, captured in ICDs for EM and Qual Model testing. Combined TVAC and thermal-balance testing of the integrated FMs will be conducted prior to S/C installation. EMC/EMI testing based on S/C requirements will be conducted on the SEB. The integrated FMs will be tested to acceptance levels. The integrated FM SEB, SCIP, and HI will be fully tested prior to S/C installation.

❑ *Contamination Control:* SECCHI's cleanliness needs and contamination control techniques will be similar to those used on the LASCO, EIT, and TRACE programs. Existing procedures and facilities are in-place to support the effort. During Phase A we will define a comprehensive contamination control program for fabrication, assembly, test, and processing activities.

1.7 Pointing and Co-Alignment. To satisfy the instrument's absolute pointing requirements, the S/C pointing must be controlled to satisfy the most stringent instrument requirement of the SECCHI suite, and COR1 presents the highest require-

Table 1-11. SECCHI Mass Summary

Unit	% Reserve	Mass w/ Reserve	Heritage			
SECCHI Electronics Box				Objective Lens	15	58
CPU CCA	-	870	SXI	Field Lens with Occulter	15	46
Memory CCA	10	451	Solar B	Doublet #1 w/Filter & Lyot Stop	15	230
S/C Interface CCA	5	378	SXI Mod	Doublet Lens #2	15	81
Housekeeping CCA	10	396	Solar B	Lens Mounts	15	115
Mechanism Controller CCAs	-	970	SXI	Rotating Waveplate	-	120
Power & Thermal Control CCA	5	693	SXI Mod	Shutter	-	125
IMC CCA	-	730	TRACE	Optical Mounts	10	213
Internal Wiring & B/P	5	1,145	SXI Mod	Inst. Harness	-	400
Enclosure (Mg)	5	1,759	SXI Mod		Subtotal	1,597
MLI and Radiator	5	420	LASCO/ MDI	CORONAGRAPH 2 (COR2)		
Main Electronics Box Total		9,131		External Occulter	-	100
Intra-Instrument Harness	-	2,500	LASCO	A0 Ring	5	105
Subtotal		11,631		Lens Mass	10	1,392
Sun Centered Instrument Package (SCIP)				Heat Rejection Mirror (Al)	5	315
SCIP Optics Box				Rotating Waveplate	-	300
Common Optical Box/Bulk-heads	15	4,543	HYTEC	Internal Occulter Assembly	15	58
Doors, One Shot Operation	5	840	LASCO	Shutter	-	125
Mounting Legs	5	735	LASCO	Filter	15	115
Sunshield (Gr/CE)	5	315	HYTEC	Optical Mounts	10	228
Alignment Cube	10	275	LASCO	Inst. Harness	-	600
Multi-Layer Insulation (MLI)	5	1,470	LASCO		Subtotal	3,337
Subtotal		8,178		Total, SCIP Common Structure & Mounts		17,021
Vector Magnetograph & Guider (VMAG)				SCIP's Camera w/ 4 CCDs		
Entrance Optics Assembly	15	138	Skylab	Camera R/O Unit (Mg)	15	1,610
Aft Optics Assembly	15	564		CCD Camera Head (4)	10	1,650
Rotating Waveplate	15	178		Be Radiator & Support (4)	10	528
Shutter	5	131	MDI, TRACE		Subtotal	3,788
Instrument Harness	-	400		Total, SCIP Instrument		20,809
Limb Sensor Pre-Amps	-	180		Heliospheric Imager (HI)		
Subtotal		1,591		HI Optics Box		
EUV Imager (EUVI)				Structure & Baffles	15	1,150
Front Filter Section	15	127		Legs	15	805
Spider Assy (inc. Sector Wheel)	15	357	TRACE/ EIT	Optics	15	230
PZT's	15	69			Subtotal	2,185
Primary Mirror Assy	15	380	TRACE	HI Camera w/ 2 CCDs		
Filter Wheel & Shutter	15	506	MDI	Camera R/O Electronics (Mg)	15	1,035
PZT Strain Gage Pre-Amps	-	180	TRACE	CCD Camera Head (2)	10	825
Inst. Harness	-	700	SXI	Be Radiator & Support (2)	10	264
Subtotal		2,318			Subtotal	2,124
CORONAGRAPH 1 (COR1)				Total, Heliospheric Imager		4,309
Straylight Baffle	5	210	GSFC	Grand Total, SECCHI Instrument Suite		36,749

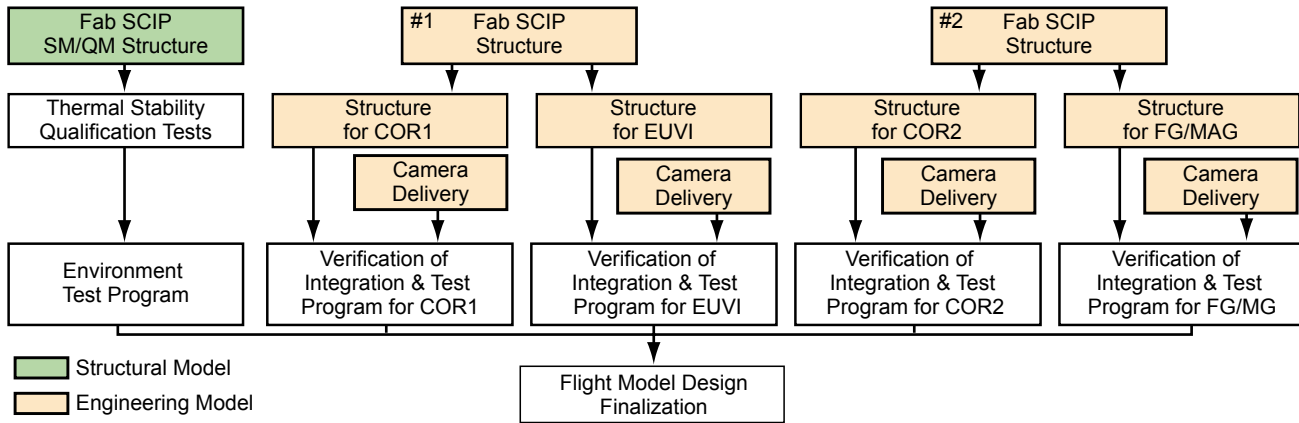


Figure 1-27. SECCHI's Engineering Model (EM) Development Approach Lowers Development Risk

ment (10 arcsec). Optical co-alignment requirements for the rest of the instruments are then determined by the absolute pointing requirements of those instruments relative to the COR1. Because the instruments with absolute pointing tolerances of less than 5 arcmin are all incorporated in the SCIP optical structure, the S/C's structural rigidity requirements, along with the complexity of the S/C level alignments and verification, are significantly reduced. This results in considerable cost and schedule savings for the S/C program.

□ **Co-alignment Approach:** An optical reference cube will be boresighted to the axis of symmetry of the HI structure and each half of the SCIP structure and mounted to the front of each. Each instrument team will integrate optics into their respective structures with the optical axis aligned with the optical reference, while addressing a second constraint to meet a focal plane axis due to the detectors and the common camera electronics. When the SCIP box halves are joined, the reference cubes on each half constrain the assembly. The most difficult of the co-alignment tasks is the relative alignment of the COR1 and COR2. In the SCIP, the coronagraphs are mounted in the same box half and will use the same alignment cube. Thus the SECCHI coronagraph co-alignment easily should be better than the LASCO alignment, which itself would satisfy SECCHI's requirements of 30" alignment (Brueckner et al. 1995).

□ **Pointing Stability:** SECCHI's stability requirements are much more stringent than the absolute pointing requirements. Techniques for isolation of both the K-corona and CMEs in the coronagraph data require pointing stability to be better than the pixel resolution because of the strong "background" intensity gradient in these instruments.

Sub-pixel stability is also important to minimize the SECCHI processor loading for sub-pixel registration in those applications requiring onboard summing. To supply this pointing, an error signal of 0.1" accuracy must be supplied to the S/C. It was demonstrated by the LASCO C2 experience that this level of pointing cannot be obtained from sensing the penumbral shadow of the external occulting disk. Therefore, a fine guide-scope is absolutely necessary. SECCHI uses fine guider electronics with demonstrated performance from TRACE and MDI.

1.8 Mission Operations. The SECCHI instrument suite is similar to the SOHO LASCO coronagraph suite (Brueckner et al., 1995) and the EIT (Delaboudiniere et al., 1995), and the SECCHI investigation incorporates "lessons learned" from those successful SOHO mission operations. Our science goals will be achieved with automated ground and flight systems that offer flexibility to the science planner, while insuring the instruments' health and welfare. Our mission operations approach is based on our experience in operating space-based solar imaging instrumentation for the successful SMM, LASCO and EIT, *Yohkoh*, and TRACE missions.

1.8.1 On-Orbit Health and Welfare. Dr. O. C. St. Cyr will be designated Lead Operations Scientist, and after launch he will be resident at GSFC in the STEREO Science Operations Center (SOC). A small cadre of SECCHI telescope operators within the SOC will perform the day-to-day hands-on mission operations. This same team will be responsible for the SECCHI health and welfare, for executing the science observing plans, and for supporting the STEREO Flight Ops Team (FOT). Our costing provided for continuing support by the

instruments' hardware and software developers. Based on our LASCO and EIT experience on SOHO, most planning and anomaly resolution can be accomplished remotely.

□ *Remote Planning and Operations:* Safe instrument operations require near-realtime monitoring, and the Internet is allowing these critical activities to take place remotely. As an example, the LASCO website (<http://lasco-www.nrl.navy.mil>) provides real-time monitoring of temperatures, voltages, and observing activities whenever instrument telemetry is being received. For SECCHI, health and welfare alerts to operators will be built into the telemetry monitoring software. Science data are automatically captured from the telemetry stream or from recorder dumps, decompressed, reformatted, assembled into time sequences, and made available online for other researchers and the public. Our experience is that this level of automation provides great flexibility while reliably maintaining the health and safety of the instruments.

□ *Flight Ops Support:* Obvious health and safety demands (voltage, temperature, and off-pointing limits) are handled by the instrument's flight software, while the S/C mission operations team is responsible for ensuring that uncontrolled full sunlight does not fall on the CCDs and other optical elements by closing a shutter before off-pointing maneuvers, and by performing periodic EUVI bake-outs to reduce contaminant deposition.

□ *Command Generation and Validation:* Command upload sequences are generated using automated tools with GUI operator interfaces. Password protection, along with special non-routine command software, prevents inadvertent transmission of critical commands. Consistent "look and feel" software display interfaces minimize operator error. Command validation is performed by: (i) the operator observing downlinked telemetry; (ii) a command file translator that converts the command load to human readable form; or (iii) automated and limited command subset built into the mission planning tools. These are the same approaches used on SOHO's LASCO, EIT, and MDI.

□ *Telemetry Displays:* We will reuse a SOHO software packet decommutator (called DDIS) that routes different data subsets to different processes (housekeeping displays, science data decompression and reformatting, archive storage, and WWW page generation) for telemetry handling. Housekeeping data are further refined into subsets with

common window displays; operators can also customize displays. A playback capability allows users to identify instrument subsystem status if on orbit anomalies occur.

1.8.2 I&T Software Reuse. We will work with the JHU/APL and GSFC to incorporate the actual ground S/W databases developed, verified, and validated during SECCHI I&T into the STEREO mission operations system. Using a single, common database in the final operations format reduces the chance of error and provides additional validation during subsystems testing with the S/C. S/W requirements include command generation, validation, and transmission; telemetry reception, translation, display, and archive for housekeeping parameters; and reception, decompression, reformatting, display, and archiving of science data.

□ *Sustaining Mission Operations:* We anticipate a smooth transition from the S/C developer to the FOT because JHU/APL performs both tasks. New interfaces between the GSFC SOC and JHU/APL are required, but this should be simplified by our use of standard protocols for passing commands, telemetry, recorder dumps, and ancillary data. Additional S/W necessary for mission operations includes a user-friendly planning and scheduling software tool (based on the LASCO and EIT planning tools) and file formats for each S/C's ephemerides and contact schedules. Other activities will be required, including the definition of science data processing. This will be based on definitive ephemerides and detector and instrumental calibrations.

1.8.3 Mission Phases. SECCHI mission operations can be divided into three phases:

□ *Phase I - Launch and Commissioning* includes a period of outgassing and CCD bake-out (for EUVI), followed by initial operations to refine and calibrate the science exposures. This phase may extend 30-45 days following launch, and parallel operations of both spacecraft may take place.

□ *Phase II - Early Cruise Phase* provides high data rate that decreases over a period estimated to be many months. Its duration depends on the selected mission profile.

□ *Phase III - Nominal Mission* begins when the S/C are sufficiently distant from the Earth that only the end-of-mission data volume is possible for a specified contact duration (5 Gbits during an 8-hour contact). This phase may start at different times for the two STEREO S/C depending on the

mission profile, but we assume that it will occur within 6-12 months following launch.

For the proposal, we baselined a synoptic program for early in Phase II that will be maintained throughout the mission. This program will meet the science objectives within the available downlink at the end of the nominal mission. During Phase II, observing sequences that require higher time cadence can be interspersed between the exposures of the synoptic program. Also, there may be periods where one or more of the SECCHI telescopes could be allocated additional resources to participate in campaigns with groundbased or other space-based platforms.

1.8.4 Autonomous Operations. On SOHO's LASCO, EIT, and MDI, proven hardware and software design approaches have maintained these instruments for over 3 1/2 years. Our experience and "lessons learned" are incorporated into the SECCHI instrument and its mission operations approach. Our instrument incorporates detailed observing sequences, mask libraries, and observing parameters as onboard macro functions triggered by an uplinked daily timeline command sequence. We baselined a low cadence, default synoptic program that executes if the daily schedule expires (perhaps due to a missed DSN contact). The default program will acquire images from each telescope at a low cadence, as long as the S/C's recorder storage is available and the instrument can be safely operated.

1.8.5 Science Planning Cycles. We baselined a STEREO planning cycle using quarterly, monthly, weekly, and daily schedules. This approach supports general guidelines and long-term constraints introduced at the quarterly meetings. Detailed timelines are constructed on a monthly basis, with a weekly schedule that is the fundamental planning unit. Daily changes require only minor modifications to the weekly schedule.

□ *Observation Planning:* The weekly schedule is the fundamental planning unit because: (i) the two spacecraft schedules need to be synchronized, which likely requires a 36-48 hour plan; (ii) the AO's limited command uplink; (iii) the inability to respond to changing solar conditions on short time scales (i.e., only daily command loads are possible); and (iv) rigid data latency requirements have not been specified, so quick-look data must suffice for routine operations.

□ *Science Planning:* Each week a Science Planner will be identified for local residency at the SOC. He/she will be responsible for that week's science plan. Working with the Lead Operations Scientist and the mission operations team, the Science Planner schedules additional onboard resources beyond those required by the synoptic program. Duties for the Science Planner include: preparation of the weekly plan during the week before execution; representing the SECCHI team at any status briefings; performing analysis of the quick-look data to ensure that scientific objectives are being satisfied; and acting as a point of contact for other ground- and space-based observers.

□ *Planning and Scheduling Tools:* The STEREO mission offers the advantage of two viewpoints, well separated from the Sun-Earth line. We have baselined planning and scheduling software that eliminates resultant temporal changes by synchronizing the schedules of both SECCHI suites to account for differences in light travel time. This offset is readily calculable given the S/C ephemerides as input data for the software tool. We anticipate that ground- and space-based observatories will obtain collaborative data sets during the mission life, and so it is important to consider synchronization with these assets.

1.8.6 Operational Constraints. The SCIP must be center-pointed to better than 2 arcsec during normal operations. There is no absolute requirement on S/C roll other than to keep the HI systems pointed at the Sun-Earth line. We prefer to keep the roll angle constant to within 30 arc seconds, with occasional off-pointing for calibration purposes. A key constraint is the need to minimize on orbit sources of contamination. The EUVI is sensitive to volatile organic materials condensing on the cold surfaces around the detector, polymerizing and degrading its UV sensitivity. The coronagraphs are sensitive to small particles attached to optical surfaces and scattering the very intense solar disk illumination.

1.8.7 Open Data Policy. Our proposal provides tightly coupled, coordinated, and optimized suite of scientific instruments to address STEREO's scientific goals. This coordination extends to the collection, analysis, and archiving of the SECCHI data that we will format and produce as both quick-look and final data versions.

□ *Coordinated System Proposal:* Additionally, we propose to incorporate into our data processing

and distribution the observations from STEREO's fields and particles experiments, and to coordinate the mission's data processing and archiving in one common effort. Through cooperative discussions, the PIETRO proposal (Len Fisk, PI) and the SWAVES proposal (J.-L. Bougeret, PI) will directly incorporate this approach. When SECCHI is accepted, we will extend this offer to all STEREO instrument providers.

□ *Data Policy:* Our STEREO mission policy will be strictly implemented. It requires that all data is made public with no more than a two month delay. With the exception of the quick-look data necessary for mission operations, all SECCHI team members are treated identically with the general community, and they will request and receive the final data in identical manners.

1.9 Data Reduction and Analysis. Our team is experienced in the coordinated data reduction and analysis of coronagraph and imaging spectrograph data based on experience with SOHO's LASCO, EIT, and MDI, as well as TRACE and *Yohkoh*. Based on this heritage, the data reduction and analysis effort for SECCHI is straightforward.

1.9.1 Data Reduction. There will be two versions of SECCHI processed data: quick-look data produced immediately for use in mission operations, and final data ready for archive.

□ *Quick-Look Data:* These data are produced from the downlinked STEREO S/C telemetry files. We baselined the use of NRL's existing science facility used on LASCO and EIT. Experiment data are downlinked from the S/C once a day, received by JHU/APL, and passed to the SOC. These data are then passed to NRL via the Internet. After receipt, we estimate that the facility's computers can reformat, decompress, and process 24 hours of observations to quick-look status within two hours, based on our experience and heritage with LASCO and EIT. Currently, it takes about 2 hours to process 24 hours of LASCO/EIT data using 1995 vintage computer systems. With the currently available computer systems, a 3x improvement to meet STEREO's needs is easily achievable. Because we must run daily models using the most recent observations, quick-look data must be processed to the same scientific level as the final data. The only difference between the quick-look data and the final data is the incorporation of the collected downlink missing data packets received from NASA. Quick-look data will be immediately available to investi-

gators. When final data are ready, the quick-look version is replaced, and the final data are archived and distributed.

□ *Final Data Product:* We baselined only one level of data for SECCHI; it includes defined data products that are immediately available via quick-look, and later final data versions. Instrument data products are image files that are flat-fielded, normalized to a one second exposure time, corrected for vignetting, geometric distortion, and stray light, and reduced by any special processing required by the telescopes, in absolute scientific units. For COR1 and COR2 we will produce B and pB images, but not the individual polarizer images. For VMAG we will produce a line-of-sight, or when full Stokes parameters are measured, a vector, photospheric magnetogram, and white light images, but not individual polarizer images. We will also run as a daily, archived modeling product, a large scale, quasi-static 3D model of the solar wind plasma and magnetic structure (WIND3D) producing B, electron density, and velocity on a defined heliospheric 3D grid.

□ *Broadcast Data Products:* We have developed algorithms for the LASCO coronagraph that detect the initiation of CMEs; for SECCHI we will set a telemetry flag to show CME initiation. We will also provide a flare flag from the EUVI images to identify and provide notification of the start of intense brightening. This may be particularly interesting for space weather if the leading westward satellite detects a flare invisible from Earth that could produce energetic particles that would travel the magnetic spiral out to Earth's position. We can incorporate in our final data file headers the instantaneous flag settings from all of the STEREO experiments to aid in data searches and as information for sorting observations in later scientific investigations.

□ *Data Formats:* Data from the five SECCHI instruments are in the format of images (readouts of CCD detectors, with choices of CCD pixel binning, readout start/end positions, filter, exposure start times, and durations), all of which are contained in the SECCHI computer's output data stream. These will be placed in the headers of the formatted data files on the ground. Data are organized as one file for one image from one instrument. The SECCHI images are naturally grouped in pairs, one from each S/C. We intend to operate the instruments in a mirrored observing plan with

identical programs for each instrument pair, but with an execution time adjustment to optimize simultaneity at the Sun when viewed from the different orbital positions. While it is not possible to view every point in space at equivalent times from two different spacecraft positions, we can optimize for Sun center for most experiments. The HI stands out, since the Sun-Earth line cannot be viewed in a simultaneous manner from both S/C. We will place into the individual file headers useful S/C telemetry information, and the exact S/C positions (using NASA orbital information files) in standard coordinates.

1.9.2 Data Retrieval and Analysis. Scientific investigators will want to group and explore the data in a wide variety of ways. The key is a database query program that returns images based on defined search criteria using selected values of the image header fields. Reduced scale GIF format images can also be accessed for preliminary evaluation. We have developed a similar query engine that is used with the LASCO and EIT data and is publicly available. We will provide a number of analysis tools, both for direct data analysis, and for scientific modeling. An analysis tool is used by an individual investigator on a selected group of data, while data products discussed earlier are produced routinely and archived. Basic data analysis tools allow the investigator to conveniently select, examine, and view the individual observations as movies. We will provide scientific analysis tools developed by the immediate experiment team and by SECCHI science team members. All programs will be compatible with Solar Software Tree standards. Table 1-12 lists some basic data and science analysis tools.

1.10 Data Archival and Data Products. We will produce quick-look and final SECCHI data products at NRL's Data Reduction and Analysis Center, which we propose to use for the STEREO Data Center (SDC). Community analysis of STEREO observations will be from a virtual center, in that data will be requested from, and delivered to, investigators via the Internet. Investigators and users will be able to perform remote data examination using the SDC computers via remote login, and can download individual observations and analysis software. We require a registration by community users, and we will maintain strict computer security measures that meet NASA guidelines. Proposal Co-Is will access the data in the

Table 1-12. Data and Scientific Analysis Tools

Calibration Tracking Tool: Instruments are characterized in the laboratory before launch and a regular observing program tracks any changes in the instrumental calibrations, especially for the EUVI. We provide a standard tool to track any calibration changes from the archived data to the most recent calibration results for any data selected by the investigator.
Correction for Cosmic Ray Blemishes: Removes cosmic ray blemishes and replacement by an average intensity from surrounding pixels.
Structure Measurement Tool: Based on existing tools developed for CME and solar wind studies by LASCO to mark structural features in successive images and produce height-time plots.
Movie Tool: Tools exist for LASCO and EIT to make multi-image, multi-telescope movies. Upgrades are planned for STEREO to allow the display of physical parameters of an axi-symmetric electron density model of the corona from pB measurements by COR1 and COR2; and for the CME column mass derived from the excess CME brightness above background from measurements made by COR1, COR2, and HI.
Potential B Field: Produces an extrapolated potential magnetic field model using a group of photospheric magnetogram images that sample the 27 day full rotational surface.
EM Tool: Provides emission measure maps from EUVI channels.
Image Visualization Tool: Provides a visualization tool to simultaneously display data from STEREO experiments.
Three-dimensional Image Reconstruction: Forms 3D reconstructions from paired STEREO images.
CME Modeling Tool: TRANS3D code models propagating CMEs.

same manner as community members. We will make no attempt to coordinate or suggest the membership of any community scientific investigation. We will request a standard acknowledgment in these papers, along with copy for the publications listing. Within the SDC, we have not proposed to provide expert guides or visitor facilities for community members, but we will provide extensive online help files and data analysis tools.

1.10.1 Data Delivery. We baselined the acquisition of our computer and storage media in the year before the STEREO mission launch. Currently, the use of DVD disks (double sided double density with 17 GBytes capacity) allow two days of STEREO observations from both satellites to be archived on one disk. We plan that the final data product will be completed within two weeks of receiving the data at the SDC given timely arrival of the downlinked data from JHU/APL. We will ensure that a secure, validated copy of the data is made before distributing final data. DVD disks will be produced at JPL from final data that is mirrored daily via the Internet. DVD disks of final data will be sent to a distribution list of interested institutions, and to the NASA Solar Data Analysis Center at GSFC for permanent archival.

1.11 SECCHI Science Team. The AO requires the listing of only individuals with critically im-

portant roles as Co-Is; it also requires the listing of funded science team member (Co-I or not). Our proposal includes 61 Co-Is and science team members. All Co-Is are providing significant support to SECCHI during the instrument development (Table 1-13). Using this approach, we are using an overage of only 5 Co-Is for each effort funded by NASA for the SECCHI instrument suite. Our rationale for this approach follows:

□ First, we proposed an instrument suite covering three of the STEREO strawman instruments plus two others. Naturally, the number of persons necessary to execute the investigation is larger; however, resource sharing results in a smaller number of participating scientists than necessary for independent proposals.

□ Second, we are receiving significant technical help from European team members whose institutional support significantly extends NASA funds devoted to the STEREO instrument and analysis efforts. Our collaborations (SOHO and *Yohkoh*) in-

volved advantageous interactions with European and Japanese Co-Is. Similarly, our European team members must be included as full SECCHI Co-Is, both for their personal recognition, and because of the institutional advantages they would lose within their national funding sources if treated unequally. We note that 22 of our Co-Is are non-U.S. individuals and not funded by NASA (see Table 1-14).

□ Third, we propose to provide a number of numerical modeling and scientific analysis tools to the community to aid in the coordinated optimal analysis of the entire STEREO set of observations. This requires the expertise of a number of individuals, funded both by NASA and by their own science agencies. The stereo nature of the observations is unique to solar observations and requires a number of new analysis tools.

□ These tools must be developed along with the instruments so as to be ready to be available before launch.

Table 1-13. SECCHI Funded Science Team

Name	Org.	Stereo Mission Role
D. Alexander	LMSAL	3D Modeling of Loops
M. Aschwanden	LMSAL	3D Modeling of Loops
R. I. Bush	NRL	Magnetograph Data Coord. Scientist
J. W. Cook	NRL	Coronagraph Data Coord. Scientist
J. M. Davila	GSFC	COR1 Project Scientist
K. P. Dere	NRL	SECCHI & HI Mission Scientist
R. R. Fisher	GSFC	COR1 Instrument Scientist
L. Golub	CfA	EUVI Consultant
J. B. Gurman	GSFC	Data Archive Coordinator
D. M. Hassler	SWRI	Coordinates Calibration Wrkg Group, IMAGE Liaison & Inst. Consultant
R. Howard	NRL	Principal Investigator
T. Hoeksema	SOG	Mission Scientist (and E/PO)
E. de Jong	JPL	3D Reconstruction Working Group
J. T. Karpen	NRL	MHD Modeling Group Coordinator
J. A. Klimchuk	NRL	MHD Modeling & Space Weather Working Groups
M. J. Koomen	NRL	Optics Scientist
C. M. Korendyke	NRL	Project Consultant
J. R. Lemen	LMSAL	LMSAL Instrument Manager
P. C. Liewer	JPL	3D Reconstruction Working Group
J. A. Linker	SAIC	MHD Modeling Working Group
T. Metcalf	LMSAL	Analysis of magnetograph data
D. J. Michels	NRL	E/PO Coordinator
J. D. Moses	NRL	SECCHI Program/EUVI Mission Scientist
J. S. Newmark	SAI	COR2 Mission Scientist
S. Plunkett	NRL	COR2 Project Scientist

Table 1-13. SECCHI Funded Science Team

Name	Org.	Stereo Mission Role
N. R. Sheeley	NRL	Modeling Group
D. G. Socker	NRL	NRL Instrument Manager, COR2 and US HI Instrument Scientist
O. C. St. Cyr	CPI	COR1 Mission/Mission Operations Scientist
T. D. Tarbell	LMSAL	Magnetograph Project Scientist
B. J. Thompson	GSFC	COR1 Data Coord. Scientist
D. F. Webb	BC	Coordinates Space Weather Modeling Group
C. J. Wolfson	LMSAL	Deputy LMSAL Instrument Manager
J-P Wülser	LMSAL	EUVI Project Scientist

Table 1-14. Other Funded Science Team Members

Name	Org.	Stereo Mission Role
S. K. Antiochos	NRL	MHD Modeling Group
D. Berghmans	R.Obs.	MHD Modeling Group
V. Bothmer	Univ. Keil	Instrument Aperture Doors, 3D Reconstruction Group
J-L H. Bourgeret	Observ. Paris	Radio Investigations Liaison
L. F. Burlaga	GSFC	MHD Modeling Group
F. Clette	ORB	Instrument Calibration & MWG
P. Cugnon	ORB	Instrument Calibration & MWG
J. L. Culhane	MSSL	CCD Camera Project Scientist
J-M Defise	CSL	HI Project Scientist for Testing
J-P Delaboudiniere	IAS	EUVI Optics Coatings & Characterization
L. A. Fisk	Univ. Mich.	Particles and Fields Liaison/MHD Modeling Group
R. A. Harrison	RAL	Camera Scientist
J-F Hochedez	ORB	Instrument Calibration & MWG
B. Inhester	MPAe	3D Reconstruction Working Group
C. Jamar	CSL	HI Instrument Test Scientist
H. Kunow	Univ. Keil	Door/3D Reconstruction Group
P. L. Lamy	LAS	COR2 Optics Consult./F Corona Modeling
J. Lang	RAL	CCD Camera Design Scientist
A. Llebaria	LAS	COR2 Optics Consult./F Coronal Modeling
E. Marsch	MPAe	Modeling Working Group
Z. Mikic	SAIC	MHD Reconstruction Working Group
M. Pick	Observ. Paris	Ground Based Radio Investigation Coordinator
P. Rochus	CSL	HI High Performance Test Instrument Scientist
R. W. Schwenn	MPAe	3D Reconstruction Working Group
G. M. Simnett	ASRG	HI Instrument Scientist
S. K. Solanki	MPAe	3D Reconstruction Working Group
A. M. Title	LMSAL	Magnetograph Scientist
T. H. Zurbuchen	Univ. Mich.	MHD Modeling Group